Geology, Geochemistry, and Geophysics of Gold-Quartz Veins in the Pistón de Uroy Area, Estado Bolívar, Venezuela

By Jeffrey C. Wynn,[1] Norman J Page,[2] Gloria Contreras,[3] R.J. Quesada,[4] Barry C. Moring,[5] *and* Robert L. Oscarson[6]

ABSTRACT

Placer mining has been active in the Pistón de Uroy area of Estado Bolívar, Venezuela, on the middle Río Chicanán since the 1940's. A recently discovered mineralized quartz-vein system in the area is hosted by a mafic-ultramafic complex emplaced in older greenstone-belt rocks of andesitic to basaltic composition. North of the mineralized area, sandstone and quartz-pebble conglomerate of the Roraima Group overlie rocks of the Early Proterozoic greenstone belts. The vein is 1–8 m or more wide and as long as 3,000 m, and it has a significant gold content, as demonstrated both by direct sampling and by the extensive placer mining activity downstream. In addition, sperrylite (a platinum-bearing mineral) is present in the ultramafic (pyroxenite) rocks. A magnetic survey shows that the pyroxenite dips moderately to the north, and very low frequency electromagnetic data were used to map faulted offsets in the quartz-vein system. Gradient-array resistivity data outline the western extension of the quartz-vein system; the vein system probably extends 700–800 m farther to the west than mapped on the surface.

RESUMEN

La minería de oro en placeres en la parte media del río Chicanán ha estado activa desde la década de 1940. Recientemente se ha descubierto un sistema mineralizado de vetas de cuarzo, las cuales están encajadas en un complejo máfico-ultramáfico que a su vez está emplazado en rocas verdes (greenstones) más antiguas de composición basaltica a andesítica. Al norte de la zona mineralizada, areniscas y conglomerados de cantos redondeados de cuarzo yacen por encima de los cinturones de rocas verdes de edad Proterozoico Temprano. La veta principal tiene 1 m de ancho y puede llegar a medir al menos 8 m de ancho, se extiende hasta 3,000 m y tiene un contenido de oro significativo, lo cual está indicado por muestreo directo y por la cantidad de actividad minera en placeres aguas abajo. Ademas, el mineral sperrylita, el cual contiene platino, está presente en las rocas ultramáficas (pyroxenita). La prospección magnética muestra que la pyroxenita está buzando moderadamente hacia el norte. La prospección electromagnética de baja frequencia (VLF) fue usada para ubicar segmentos fallados en el sistema de vetas de cuarzo. "Gradient array resistivity data" revelan que el sistema de vetas de cuarzo se extiende entre 700 y 800 m más hacia el oeste que lo indicado en superficie.

INTRODUCTION

The Pistón de Uroy area is southwest of El Dorado in Estado Bolívar, north of the Río Chicanán between lat 6°15′ and 6°20′ N. and long 61°51′ and 61°56′ W. (fig. 1). Access to the area is either by air or river; roads to the area do not exist.

Placer deposits of gold have been exploited on the Río Chicanán and its tributaries near Pistón de Uroy since the 1940's, thus indicating that the area might contain lode sources of gold. During regional reconnaissance, gold was identified in alluvial deposits in the La Franela stream channel and elsewhere in the Pistón de Uroy area, and a complex suite of mafic and ultramafic rocks was identified that is overlain unconformably by sedimentary rocks of the Early to Middle Proterozoic Roraima Group (Alberdi, 1988). Subsequently, in March and November 1988 and February and May 1989, N.J Page, G. Contreras, J.C. Wynn, D. Freitas, J. Quesada, and L. Guilloux conducted the fieldwork that

[1]U.S. Geological Survey, Unit 62101, APO AE 09811-2101, USA

[2]U.S. Geological Survey, Corbett Building., 210 E. 7th Street, Tucson, Arizona 85705.

[3]Voie de la Croix, 55000 Behonne, France; formerly Corporación Venezolana de Guayana, Técnica Minera, C.A., Puerto Ordaz, Venezuela.

[4]Urbanización Quebrada de Cariaco, Calle Llamo Adentro, No. 276, Municipio Vargas, Caracas, Venezuela; formerly Corporación Venezolana de Guayana, Técnica Minera, C.A., Puerto Ordaz, Venezuela.

[5]U.S. Geological Survey, 345 Middlefield Road, MS984, Menlo Park, California 94025.

[6]U.S. Geological Survey, 345 Middlefield Road, MS916, Menlo Park, California 94025.

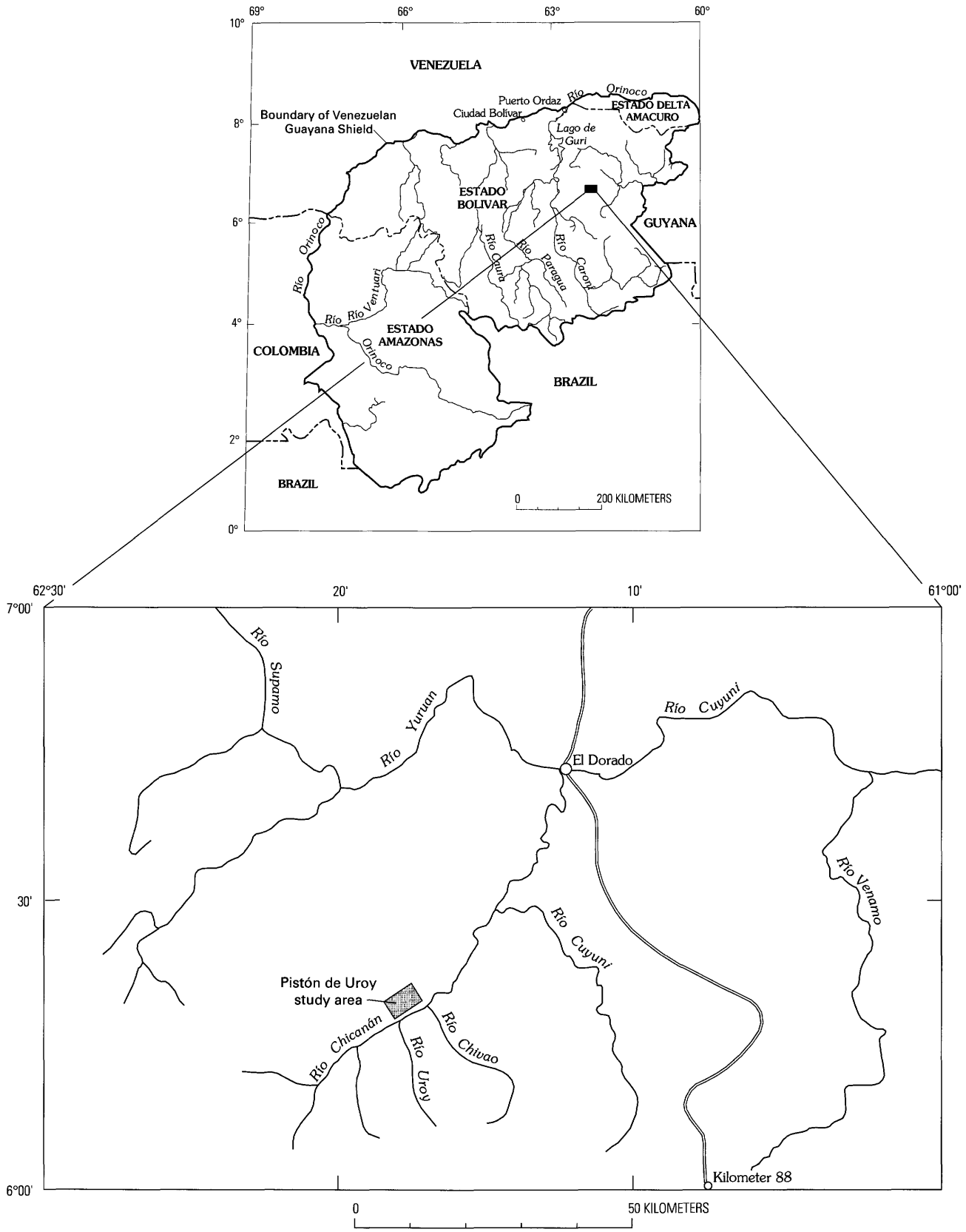

Figure 1. Maps showing location of the Pistón de Uroy study area, Estado Bolívar, Venezuela.

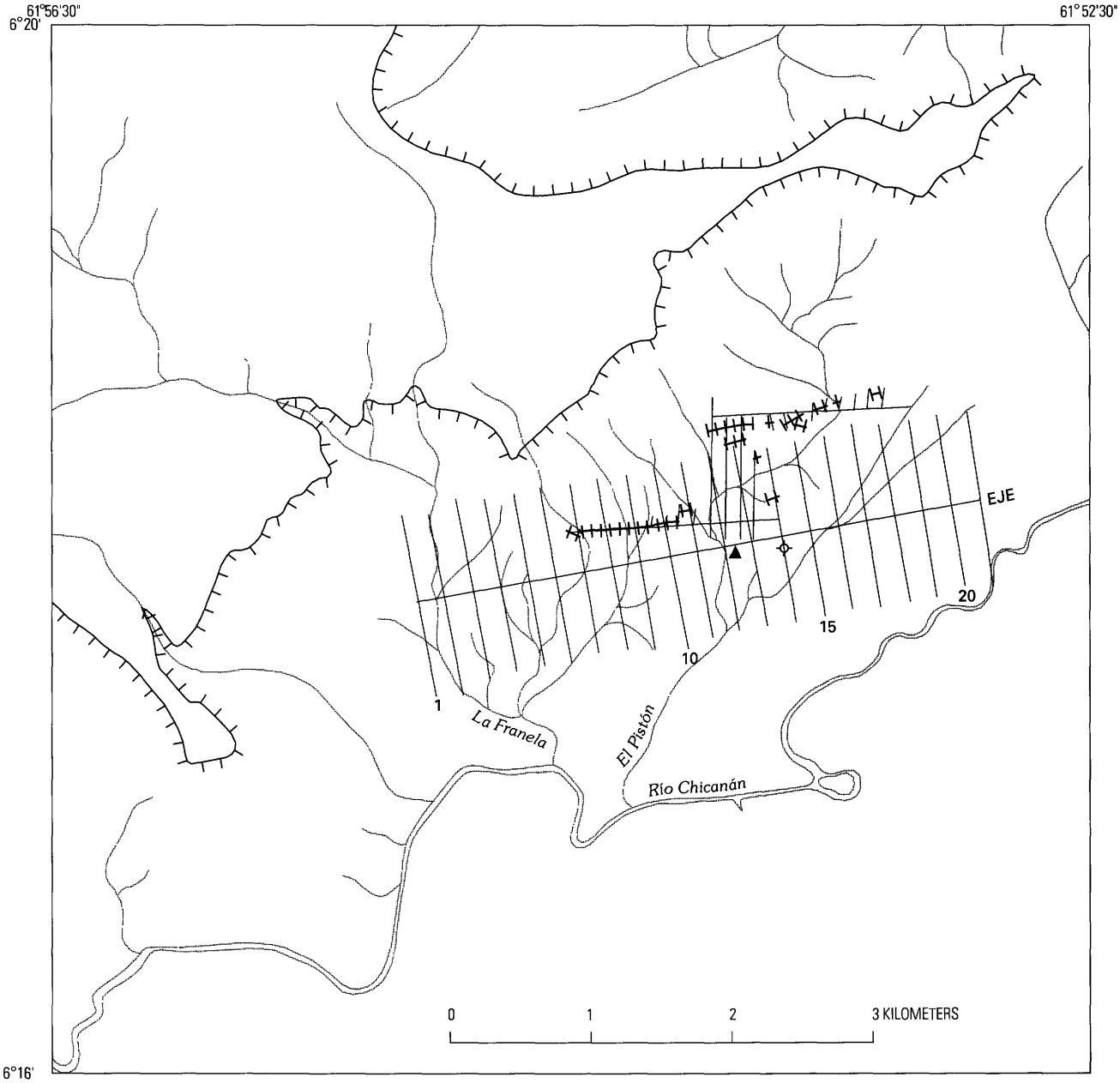

Figure 2. Map showing the quartz-vein system (railroad tracks), geologic grid (smaller, east-west grid parallel with the quartz-vein system), and geophysical grid (larger, regular grid with eje (baseline) trending N. 80° E. and picas trending north-northwest and numbered from east to west), Pistón de Uroy area, Venezuela. The geophysical camp is shown by a triangle and the local heliport as a circle with four tick marks.

forms the basis for this report. Although some outcrops are present in the drainages and on ridges in the area, the area is heavily forested, and much of the study was conducted using cleared paths or profiles (called picas) at 100-m intervals perpendicular to axes that are subparallel with the strike of the vein structure and the geologic units. The location of the geophysical and geological grids established in the study area and the location of the quartz-vein system are shown in figure 2. Within the context of the regional geology, which is not well known, the structure, lithology, petrology, and geochemistry of the gold-quartz veins and their host rocks in the Pistón de Uroy area are described. Because of the extensive soil and jungle coverage of the area, resistivity, magnetic, and very low frequency electromagnetic geophysical techniques were used to better define the geology.

GEOLOGY

The Pistón de Uroy area forms part of an extensive greenstone belt in which rocks of the Pastora Supergroup

and the younger Botanamo Group have been reported (Mendoza, 1977; Tosiani and Sifontes, 1989). To the north, between the Río Chicanán and the town of El Dorado, Tosiani and Sifontes (1989) identified gabbro, pyroxenite, and olivine cumulates. More recent work (Floyd Gray, U.S. Geological Survey, oral commun., 1990) confirms the existence of mafic and ultramafic cumulates in this area. This mafic-ultramafic complex was emplaced into andesitic and more siliceous volcanic rocks. Areas east and northeast of Pistón de Uroy are underlain by basaltic and andesitic volcanic rocks intruded by granitic rocks of the Supamo Complex. The greenstone-granite terrane is overlain by rocks of the Roraima Group (Alberdi and Contreras, this volume).

Folded flows, tuffs, and volcaniclastic rocks of andesitic to basaltic composition form the country rocks of a mafic-ultramafic complex that is host to the mineralized quartz-carbonate veins north of Río Chicanán (plate 1). Both groups of rocks are cut by diabase dikes; in addition, the mafic-ultramafic complex is cut by basaltic to andesitic brecciated and porphyritic dikes that are locally mineralized with pyrite and chalcopyrite. These volcanic and plutonic rocks underlie the relatively low (50–100 m relief), rounded hills north of the river. The steep escarpment farther to the north is formed by unconformably overlying rocks of the Roraima Group including sandstone, quartzite, conglomerate, and interlayered mudstone. Extensive colluvial and alluvial deposits cover much of the pre-Roraima Group bedrock, and close to the escarpment large blocks of quartzite, some as big as houses, form talus piles. Major structural features in the area include faults and east-striking quartz veins; the veins are cut by north-northwest-striking faults. On the southeast side of the mafic-ultramafic complex, veins and faults are cut by a northeast-striking fault filled by a diabase dike.

The mafic-ultramafic complex is composed of layered cumulus dunite, wehrlite, and clinopyroxenite and locally foliated, laminated, generally homogeneous gabbro. Layering and lamination strike northwest and dip to the north; modal-, phase-, and size-graded layering are present in the ultramafic rocks. Locally, the gabbro forms phase layers of two-pyroxene plagioclase cumulate and plagioclase cumulate containing oikocrysts of pyroxene. The ultramafic rocks are composed of varying proportions of cumulus olivine, chromite, and clinopyroxene and postcumulus plagioclase, orthopyroxene, and brown hornblende. Textures are generally well preserved; however, the primary minerals are partly to totally altered to mixtures of serpentine minerals, talc, amphiboles, and magnetite. Accessory sulfide minerals include chalcopyrite, pyrrhotite, and pyrite; chalcopyrite is the most abundant sulfide mineral in clinopyroxene cumulates.

Olivine and olivine-chromite cumulates contain euhedral to subhedral olivine altered to serpentine minerals and magnetite, accessory amounts of pyrrhotite, chalcopyrite, and pyrite, and euhedral chromite that has secondary magnetite rims. Locally, oikocrysts of orthopyroxene are altered to talc, amphibole, and serpentine minerals. Most of the sulfide minerals are in interstitial spaces or at the margins of cumulus crystals, but rare inclusions of pyrrhotite and chalcopyrite in chromite are present.

Clinopyroxene cumulates consist of euhedral to subhedral, cumulus clinopyroxene that is locally twinned, has spinel exsolution lamellae, and is replaced to some degree by postcumulus brown amphibole. Interstitial postcumulus plagioclase is altered to tremolite-actinolite, chlorite, epidote, clay, and possible zeolite minerals. Some rocks contain oikocrysts of orthopyroxene altered to serpentine minerals and tremolite-actinolite. Primary brown hornblende is present interstitially. Euhedral to subhedral magnetite having exsolution lamellae of ilmenite (?) is also a primary magmatic mineral; both the magnetite and ilmenite are altered to secondary iron oxide minerals. One sample contained both interstitial biotite altered to chlorite and quartz associated with sulfide clots.

Secondary minerals in the clinopyroxene cumulates include green-brown to colorless amphibole that locally forms radiating clusters of crystals, as well as talc, chlorite, magnetite, epidote, and serpentine minerals. Sulfide minerals such as pyrrhotite, chalcopyrite, and pyrite are present as either single- or multi-phase grains and form inclusions in primary magnetite and clinopyroxene; they also are present in interstitial spaces. During the development of secondary amphiboles and other alteration minerals, the sulfide minerals were remobilized to varying degrees and formed intergrowths with the amphiboles. In the more altered rocks, pyrrhotite and chalcopyrite are replaced marginally and along fractures by magnetite. Sparse clusters of pyrite crystals, as much as 1 mm in diameter, are present. In these clusters, chalcopyrite and pyrrhotite are present both as inclusions in individual pyrite crystals and as interstitial material between pyrite crystals.

Clinopyroxene-olivine, clinopyroxene-orthopyroxene, and clinopyroxene-olivine-chromite cumulates are also present in the mafic-ultramafic complex. Primary and secondary minerals have the same cumulus and alteration textures as in the single-phase cumulates. The clinopyroxene-olivine-chromite cumulate contains only traces of pyrite, and the clinopyroxene-olivine cumulate contains only traces of pyrrhotite and chalcopyrite. These two latter types of cumulates are notably deficient in sulfide minerals in comparison with other cumulates.

The mafic part of the complex consists of plagioclase-clinopyroxene cumulates and minor amounts of plagioclase-clinopyroxene-orthopyroxene and plagioclase cumulates; all three rock types are locally laminated and modally layered. The plagioclase-clinopyroxene cumulate is composed of euhedral to subhedral cumulus plagioclase and clinopyroxene; postcumulus brown hornblende fills interstitial spaces and replaces clinopyroxene. Primary magnetite is also present. Secondary alteration minerals include variously colored amphiboles, chlorite, and epidote. Chalcopyrite,

Table 1. Trace-element and platinum-group-element analyses of unmineralized rocks from the Pistón de Uroy area, Venezuela.

[Location of samples shown by number on plate 1. Semiquantitative six-step emission spectrographic analyses are in parts per million except for Ti, which is in percent; analyst, R. Hopkins. Fire-assay inductively coupled mass spectrometry analyses are in parts per billion; analysts, P. Aruscavage and G. Riddle. Elements looked for but not detected at levels indicated given (in parts per million): Ag (0.5), As (200), Au (10), Be (1), Bi (10), Cd (20), Ge (10), La (50), Mo (5), Nb (20), Sb (200), Th (100), W (20), and Zn (200). N indicates not detected at level shown]

	UGP–1	UGP–3	UGP–5	UGP–8	UGP–14	UGP–17	UGP–25	UGP–28	UGP–29	UGP–30	UGP–35	UGP–36	UGP–37	UGP–38	UGP–39	UGP–44[1]
Semiquantitative emission spectrography																
Ti	0.3	0.2	0.3	0.15	0.5	0.5	0.7	0.5	0.3	0.3	0.2	0.15	0.3	1.0	0.5	0.3
B	15	10	10	N10	15	<10	20	10	10	10	10	10	<10	<10	10	10
Ba	1,500	50	N20	N20	20	<20	1,500	20	<20	20	20	20	N10	70	<20	200
Co	15	200	200	30	300	100	70	70	200	70	70	70	100	70	70	70
Cr	70	5,000	1,500	700	5,000	3,000	1,000	1,500	1,500	1,000	50	50	1,000	30	3,000	700
Cu	30	10	30	15	70	50	15	300	70	300	300	200	30	70	50	70
Ga	30	10	10	5	7	7	20	10	10	10	20	15	10	20	10	15
Mn	700	1,000	1,000	700	1,000	1,000	1,000	1,500	1,500	1,000	1,000	1,000	1,000	1,000	1,500	1,000
Ni	30	1,500	300	100	1,500	700	200	300	700	200	150	150	200	30	200	150
Pb	30	<10	<10	N10	N10	N10	15	N10	N10	<10	<10	<10	<10	10	N10	N10
Se	10	10	50	15	15	50	30	50	30	30	30	20	30	20	30	20
Sr	500	N100	N100	N100	N100	N100	500	N100	N100	150	300	300	N100	300	N100	300
V	100	150	150	70	200	150	150	150	100	100	150	100	150	300	150	150
Y	15	N10	15	<10	<10	15	20	15	10	15	10	<10	15	20	20	10
Zr	100	N10	20	10	10	20	100	30	15	10	10	10	30	100	15	15
Inductively coupled mass spectrometry																
Pt	<0.5	13	86	1.5	1.8	250	9.2	1.5	<0.5	1.0	0.9	0.6	0.6	170	170	0.5
Pd	<0.8	16	39	8.0	17	260	12	2.3	1.1	0.9	1.3	2.6	<0.8	100	190	1.3
Rh	<0.5	0.6	12	<0.5	0.8	21	0.7	<0.5	<0.5	<0.5	<0.5	<0.5	<0.5	25	15	<0.5
Ru	<0.5	20	19	<0.5	13	41	0.9	<0.5	<0.5	<0.5	<0.5	<0.5	<0.5	22	30	<0.5
Ir	<0.5	3.5	10	<0.5	3.0	18	<0.5	<0.5	<0.5	<0.5	<0.5	<0.5	<0.5	14	13	<0.5

Sample descriptions

UGP–1	Porphyritic andesite, altered	UGP–29	Clinopyroxene cumulate, altered
UGP–3	Olivine-chromite cumulate, serpentinized	UGP–30	Clinopyroxene-orthopyroxene cumulate
UGP–5	Cinopyroxene cumulate	UGP–35	Clinopyroxene-plagioclase cumulate
UGP–8	Clinopyroxene cumulate, altered	UGP–36	Clinopyroxene-plagioclase cumulate
UGP–14	Olivine-pyroxene-chromite cumulate, serpentinized	UGP–37	Clinopyroxene cumulate
UGP–17	Clinopyroxene-plagioclase(?) cumulate, altered	UGP–38	Clinopyroxene-olivine cumulate
UGP–25	Volcanic rock, totally altered	UGP–39	Clinopyroxene cumulate, altered
UGP–28	Clinopyroxene cumulate	UGP–44	Plagioclase-clinopyroxene cumulate, laminated

[1]Contains 3 ppm Ag.

pyrrhotite, and pyrite are present interstitially, and their intergrowth with secondary amphiboles indicates some degree of remobilization of elements in the sulfide minerals during alteration. Locally, pyrite is present as sparsely distributed single crystals as much as 2 mm in size. In more altered rocks, both chalcopyrite and pyrrhotite are replaced by magnetite, and covellite and chalcocite locally replace chalcopyrite.

The quartz-vein system was mapped in detail between the El Pistón drainage and slightly west of the La Franela drainage (fig. 2, plate 1). The veins generally strike approximately east and dip steeply south or north. The veins and bands of altered country rock are 1–8 m wide. Outcrops are sparse in the area; the veins are marked only by blocks of quartz, rare outcrops, and, in places, extensive float. Where outcrop was sufficient, profiles perpendicular to the width of the vein were described, measured, and sampled by chipping across the profile over a measured thickness (plate 1). Elsewhere, chip samples from blocks were collected; sampling was biased toward the more oxide stained parts of the blocks. The contact between gabbro and ultramafic rocks was not observed but was mapped using geophysical information (Quesada and Wynn, 1990).

Quartz-vein material is present in four different geological settings (plate 1): (1) near the southern contact between gabbro and the ultramafic rocks; for example, from east of the La Franela drainage to 0+430 W on the southern eje; (2) near the northern contact between gabbro and ultramafic rocks; for example, between 0+150 and 0+650E on the northern eje; (3) in gabbro; for example, between 1+100 and 1+100E on southern eje; and (4) in ultramafic rocks; for example between 0+500 and 1+000E on the northern eje. As shown in the cross sections (plate 1), the characteristics of the veins change along their strike and across their width. For example, in outcrops along the La Franela drainage (see profile, plate 1), the vein system consists of several thin (as thick as 20 cm) quartz veins and quartz stockwork over a width of about 5 m in sheared and highly altered ultramafic rocks consisting of talc and serpentine, carbonate, and iron oxide minerals. East of La Franela, the vein is represented by 2–5-m-wide blocks of white quartz or quartz and oxidized material. In general, veins in ultramafic rocks contain less quartz by volume than veins in gabbroic rocks.

The vein material includes white, massive, barren quartz; quartz-carbonate; gray quartz; manganese-iron-oxide-brecciated quartz; and vuggy quartz crystals. Alteration minerals consist of talc, amphiboles (?), chlorite, and serpentine, carbonate, and iron oxide minerals in highly sheared rock. All of the surface exposures are oxidized and apparently leached. Sulfide minerals were found only in vein material from a dump of an exploration adit at the eastern end of the vein system.

The veins formed in shear zones, near lithologic contacts or in faults, that strike approximately east. This early generation of structures is cut by faults that trend

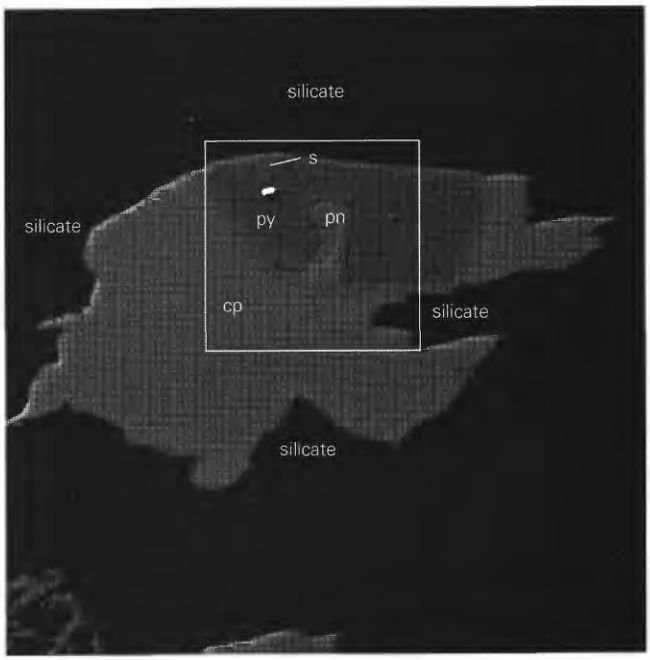

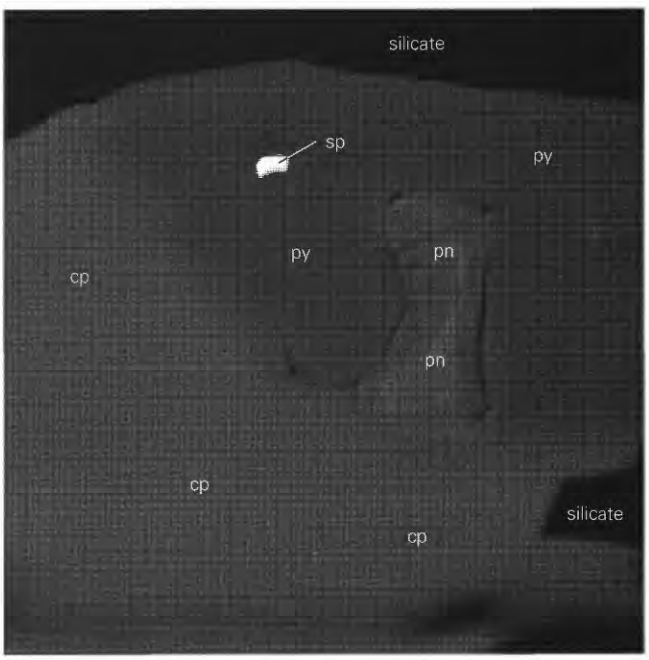

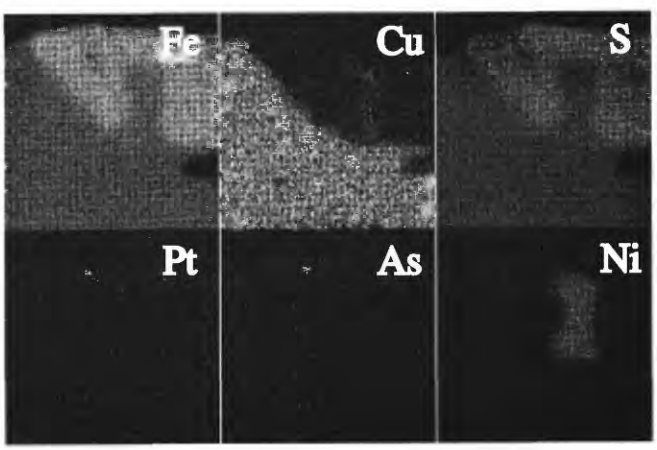

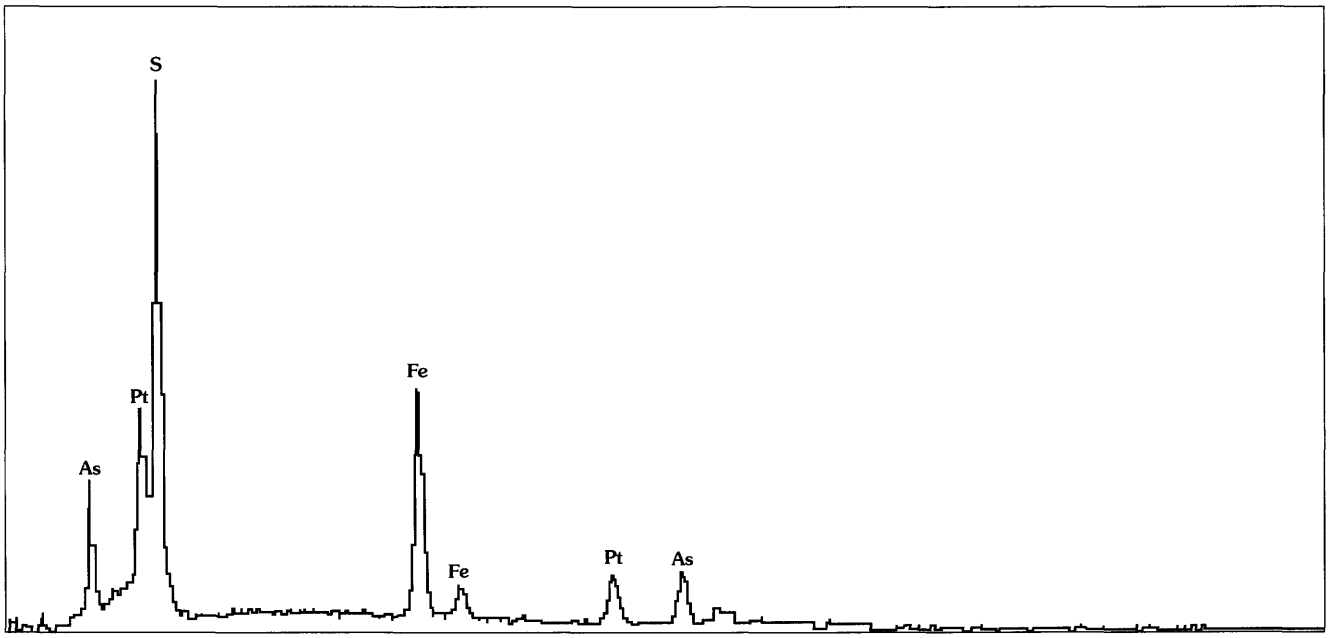

Figure 3 (above and facing column). Scanning electron microprobe images and spectrum of sperrylite in a composite grain of pyrite-chalcopyrite in altered clinopyroxenite, sample UGP–39, Pistón de Uroy area, Venezuela. *A–C*, Backscattered electron images. White area, sperrylite (s); light-gray areas, chalcopyrite (c) and pentlandite (pn); medium-gray area, pyrite (py); black area, silicate minerals. *B* is an enlargement of the area in *A* that is shown by the box. *C*, Images for iron, copper, sulfur, platinum, arsenic, and nickel. *D*, Spectrum from the sperrylite grain.

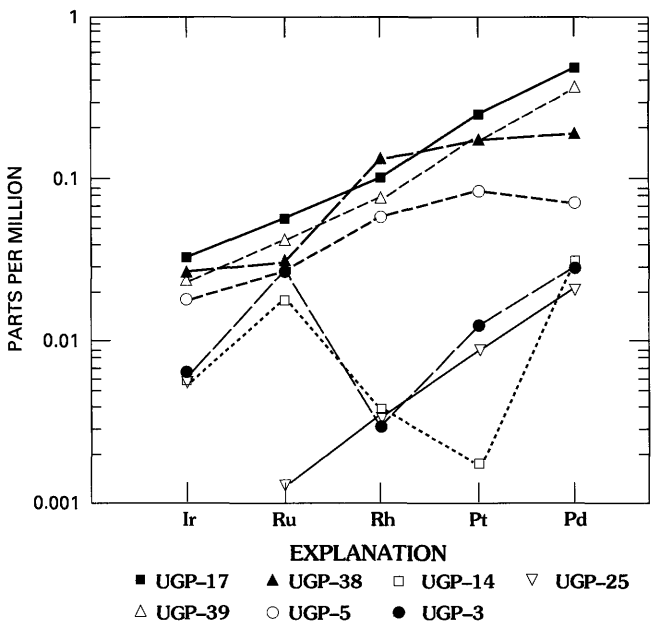

Figure 4. Chondrite-normalized patterns for clinopyroxene (UGP–39, UGP–5), clinopyroxene-olivine (UGP–38), clinopyroxene-plagioclase (UGP–17), olivine-chromite (UGP–3), and olivine-clinopyroxene-chromite (UGP–14) cumulates and a sample of volcanic rock (UGP–25), Pistón de Uroy area, Venezuela. Values used for normalization are from Naldrett (1981).

north-northwest and offset the veins. These faults are cut by a third generation of structures that probably are major regional shear zones, such as the faults causing the El Pistón drainage, and are clearly visible in the very low frequency electromagnetic data (described later in this chapter).

GEOCHEMISTRY

A variety of materials was sampled during the course of the study. Panned concentrates were examined visually for gold (plate 1, VP-number series). In drainages that cross the vein system, samples collected below the veins contain gold. One hundred and nineteen samples of vein material, soil, and weathered adjacent rock were analyzed by semiquantitative six-step emission spectrography (Grimes and Marranzino, 1968) and for platinum-group elements by fire-assay inductively coupled plasma mass spectrometry (Meier and others, 1988). Vein materials and soils were analyzed for Se by hydride-generation atomic absorption, for Te and Ti by flameless atomic absorption, for Hg by cold-vapor atomic absorption, for F by specific-ion electrode, for Au by graphite-furnace atomic absorption, and for As, Bi, Cd, Sb, and Zn by inductively coupled plasma; methods are described by O'Leary and Meier (1986). Table 1 presents analytical results for unmineralized rocks and table 2 analytical results for vein material, soil, and weathered rock samples.

Table 2. Gold and trace-element analyses of rock and soil samples from quartz veins in the Pistón de Uroy area, Venezuela.

[Location of samples shown by number on plate 1. In parts per million except for Au, which is in parts per billion. N indicates not detected at level shown; leaders (--) indicate no data available. Analysts: R. Hopkins, P. Hageman, E. Welsch, F. Tippih, J. Shankey, D. Fey]

	V1	V2	V3	V4	V5	V6	V7	V8	V9	V10	V11A	V11B	V12
Gold and trace elements by various methods													
Au	7	42	<2	<2	4,640	320	25	<2	<2	<2	<2	20	600
As	100	1.0	0.4	4.8	5.5	170	1.8	18	0.2	35	1.3	4.1	54
Cd	--	--	--	--	--	--	--	--	--	--	--	--	--
Hg	<0.02	<0.02	<0.02	<0.02	<0.02	<0.02	<0.02	<0.02	0.02	<0.02	<0.02	0.08	0.02
Sb	--	--	--	--	--	--	--	--	--	--	--	--	--
Se	0.3	<0.1	<0.1	0.1	0.2	0.4	<0.1	<0.1	<0.1	0.2	<0.1	0.1	0.3
Te	<0.05	<0.05	<0.05	<0.05	0.05	0.05	<0.05	<0.05	0.15	<0.05	<0.05	1.3	<0.05
Tl	<0.05	<0.05	<0.05	<0.05	0.20	0.15	<0.05	<0.05	<0.05	<0.05	<0.05	0.60	<0.05
Zn	--	--	--	--	--	--	--	--	--	--	--	--	--
Semiquantitative emission spectrography													
Ag	N0.5	N0.5	N0.5	N0.5	N0.5	N0.5	N0.5	N0.5	N0.5	N0.5	N0.5	N0.5	N0.5
Ba	20	30	20	<20	700	30	20	<20	20	<20	<20	700	<20
Co	200	N10	N10	N10	500	200	<10	30	N10	20	N10	300	50
Cr	1,000	15	30	30	20	1,000	70	700	20	100	20	700	1,000
Cu	50	<5	N5	10	300	300	30	50	7	20	7	700	100
Mn	1500	30	10	15	>5,000	1,000	500	200	50	500	150	>5,000	700
Ni	2,000	7	<5	<5	150	150	7	100	<5	50	5	300	50
Pb	10	N10	N10	N10	<10	15	N10	N10	20	N10	N10	10	<10
V	100	<10	15	30	50	150	30	150	20	30	15	70	100

	V13	V14	V15	V16	V17	UV-1-89	UV-2-89	UV-3-89	UV-4-89	UV-5-89	UV-6-89	UV-7-89	UV-8-89
Gold and trace elements by various methods													
Au	60	1100	220	<2	<2	84	40	<2	6	6	<2	<2	950
As	87	430	210	4.6	8.2	1,310	170	<5	<5	12	13	77	161
Cd	--		--	--	--	0.7	0.4	<0.1	<0.1	<0.1	<0.1	0.9	1.0
Hg	<0.02	<0.02	<0.02	<0.02	<0.02	0.20	0.02	N0.02	N0.02	N0.02	N0.02	0.02	0.02
Sb	--	--	--	--	--	6.0	2	<2	4	<2	<2	<2	<2
Se	0.8	0.9	0.3	0.5	0.3	5.8	1.6	<0.2	<0.02	0.2	<0.02	0.7	0.3
Te	<0.05	0.25	<0.05	<0.05	<0.05	0.4	0.05	<0.05	0.10	<0.05	<0.05	0.10	0.15
Tl	0.60	0.15	0.15	<0.05	<0.05	0.15	0.10	<0.05	<0.05	<0.05	<0.05	0.20	0.15
Zn	--	--	--	--	--	40	40	7	53	11	16	101	35
Semiquantitative emission spectrography													
Ag	N0.5	N0.5	N0.5	N0.5	N0.5	N0.5	N0.5	N0.5	N0.5	N0.5	N0.5	N0.5	N0.5
Ba	<20	<20	70	30	20	70	50	100	300	70	100	300	300
Co	20	70	150	30	N10	50	50	50	300	30	30	300	500
Cr	300	700	1,500	200	70	1,000	700	50	50	100	150	700	1,000
Cu	50	50	100	15	15	70	70	30	700	50	50	700	700
Mn	300	700	1,000	700	100	1,500	1,000	1,500	>5,000	1,500	1,500	>5,000	>5,000
Ni	100	500	500	30	7	300	200	70	700	50	100	300	200
Pb	<10	10	10	N10	<10	15	20	N10	N10	N10	N10	15	15
V	50	70	100	70	20	150	100	30	100	70	70	200	150

	UV–9–89	UV–10–89	UV–11–89	UV–12–89	UV–13–89	UV–14–89	UV–15–89	UV–16–89	UV–17–89	UV–18–89	UV–19–89	UV–20–89	UV–21–89
Gold and trace elements by various methods													
Au	14	12	22	38	1,400	400	22	22	350	1,600	42	650	12
As	15	<5	7	<5	9	33	21	57	43	19	51	44	20
Cd	<0.1	<0.1	<0.1	<0.1	1.2	1.3	0.4	2.0	0.7	0.8	1.7	1	0.6
Hg	N0.02	0.02	N0.20	0.02	N0.20	1.7	0.04	0.04	0.06	0.02	0.04	0.08	0.08
Sb	<2	<2	<2	<2	<2	<2	<2	<2	<2	<2	<2	<2	<2
Se	<0.02	<0.02	<0.02	<0.02	<0.02	0.20	0.9	0.9	1.2	<0.2	0.4	1.4	0.9
Te	<0.05	<0.05	<0.05	<0.05	<0.05	0.15	0.05	0.20	0.10	0.05	0.15	0.30	0.25
Tl	<0.05	<0.05	<0.05	<0.05	0.30	0.40	0.25	0.10	0.20	0.05	0.20	0.10	0.10
Zn	2	<2	4	2	55	35	5	39	18	37	46	27	16
Semiquantitative emission spectrography													
Ag	N0.5	N0.5	7	N0.5	<0.5	0.5	N0.5	N0.5	N0.5	N0.5	N0.5	N0.5	N0.5
Ba	20	50	70	30	700	200	200	70	200	20	200	70	70
Co	<10	70	100	70	300	30	N10	70	30	30	50	30	15
Cr	70	20	50	50	70	500	200	700	200	50	200	200	200
Cu	30	30	70	30	300	200	100	300	150	150	200	100	100
Mn	200	1,500	1,500	1,000	>5,000	300	150	200	200	200	200	300	150
Ni	10	30	30	20	100	50	70	70	70	50	100	50	50
Pb	N10	N10	N10	N10	N10	15	15	15	15	10	15	15	15
V	30	30	30	30	50	150	1 50	150	150	70	100	150	150

	UV–22–89	UV–23–89	UV–24–89	UV–25–89	UV–26–89	UV–27–89	UV–28–89	UV–29–89	UV–30–89	UV–31–89	UV–32–89	UV–33–89	UV–34–89
Gold and trace elements by various methods													
Au	950	120	300	350	4	42	200	4200	14	20	16	2	10
As	20	26	20	32	24	<5	366	46	140	84	123	44	99
Cd	0.9	0.9	1.2	0.9	<0.1	<0.1	0.9	2.6	1.8	0.4	1.6	0.3	1.4
Hg	0.06	0.04	0.02	0.04	0.04	N0.02	N0.02	0.04	N0.02	N0.02	0.02	N0.02	N0.02
Sb	<2	<2	<2	<2	<2	<2	<2	<2	<2	<2	<2	<2	<2
Se	1.2	0.8	0.2	0.7	0.8	0.3	1.5	1.0	<0.2	<0.2	<0.2	<0.2	<0.2
Te	0.20	0.10	<0.05	0.10	0.05	<0.05	0.20	0.35	0.05	<0.05	<0.05	<0.05	<0.05
Tl	0.20	0.25	0.20	0.20	0.05	0.05	0.05	0.15	<0.05	<0.05	0.05	<0.05	0.05
Zn	23	19	36	25	4	<2	51	57	111	107	160	112	116
Semiquantitative emission spectrography													
Ag	N0.5	N0.5	N0.5	N0.5	N0.5	N0.5	N0.5	N0.5	N0.5	N0.5	N0.5	N0.5	N0.5
Ba	150	200	200	200	70	30	30	100	150	200	500	50	300
Co	30	30	70	50	<10	N10	30	70	100	100	150	50	150
Cr	500	300	150	300	150	100	500	1,000	2,000	2,000	2,000	700	2000
Cu	300	500	300	300	50	10	50	150	70	150	50	100	300
Mn	300	300	200	500	300	150	700	1,500	1,500	1,500	1,500	700	1500
Ni	70	70	100	100	50	7	150	300	500	500	700	300	700
Pb	15	15	10	15	<10	<10	15	15	15	<10	<10	<10	<10
V	200	200	150	200	100	70	100	150	150	150	150	100	150

Table 2. Gold and trace-element analyses of rock and soil samples from quartz veins in the Pistón de Uroy area, Venezuela—Continued.

	UV-35-89	UV-36-89	UV-37-89	UV-38-89	UV-39-89	UV-40-89	UV-41-89	UV-42-89	UV-43-89	UV-45-89	UV-46-89	UV-47-89	UV-48-89
Gold and trace elements by various methods													
Au	10	4	8	10	2	8	2	300	16	28	<2	10	10
As	68	48	47	109	304	182	<5	10	6	8	13	51	12
Cd	1.4	1.9	<0.1	1.2	0.7	0.5	<0.1	<0.1	<0.1	<0.1	<0.1	1.4	<0.1
Hg	N0.02	N0.02	N0.02	N0.02	0.02	0.02	0.02	0.04	N0.02	0.02	N0.02	N0.02	N0.02
Sb	<2	<2	<2	<2	4	<2	<2	<2	<2	<2	<2	<2	<2
Se	<0.2	<0.2	<0.2	<0.2	0.3	0.4	0.2	0.3	<0.2	1.2	<0.2	0.5	<0.2
Tl	<0.05	<0.05	<0.05	<0.05	0.05	0.10	<0.05	0.10	<0.05	0.05	<0.05	0.05	<0.05
Ti	0.10	0.05	<0.05	<0.05	0.15	0.05	0.05	0.10	<0.05	<0.05	<0.05	0.75	<0.05
Zn	92	116	25	73	58	40	2	2	<2	31	7	196	<2
Semiquantitative emission spectrography													
Ag	N0.5	N0.5	N0.5	N0.5	N0.5	N0.5	N0.5	0.7	N0.5	N0.5	N0.5	7	N0.5
Ba	300	500	100	150	200	20	30	30	70	<20	20	5,000	70
Co	100	150	70	200	100	30	<10	30	N10	70	<10	1,000	15
Cr	2,000	3,000	2,000	5,000	700	700	100	500	70	1,500	150	150	100
Cu	200	100	200	300	50	30	30	300	20	70	50	1000	30
Mn	1,500	1,500	700	1,000	1,500	1,000	500	1,000	300	1,500	300	>5,000	1,000
Ni	700	700	500	1,000	150	100	30	150	7	200	30	300	7
Pb	<10	<10	<10	<10	10	<10	<10	N10	N10	N10	N10	15	N10
V	150	150	150	200	150	150	30	100	30	100	70	150	50
	UV-49-89	UV-50-89	UV-51-89[1]	UV-52-89[2]	UV-53-89[3]	UV-54-89	UV-55-89	UV-56-89	UV-57-89	UV-58-89	UV-59-89	UV-60-89	UV-61-89
Gold and trace elements by various methods													
Au	<2	<2	2	10	68	22	30	6	14	<2	<2	<2	<2
As	26	12	62	49	64	270	295	245	38	20	9	6	<5
Cd	<0.1	<0.1	<0.1	0.1	0.2	0.2.	0.2	0.2	0.1	0.4	0.7	0.6	0.2
Hg	N0.02	N0.02	0.08	0.02	0.02	N0.02	N0.02	0.02	N0.02	0.02	0.02	0.02	0.02
Sb	<2	<2	2	3	<2	3	<2	3	<2	<2	<2	<2	<2
Se	0.6	<0.2	<0.2	0.3	0.3	<0.2	0.3	0.6	<0.2	0.7	0.5	0.4	<0.2
Tl	0.10	<0.05	0.30	0.10	0.10	0.10	0.05	0.10	0.15	<0.05	<0.05	<0.05	<0.5
Ti	<0.05	<0.05	<0.05	<0.05	<0.05	<0.05	<0.05	<0.05	<0.05	0.05	<0.05	<0.05	<0.05
Zn	<2	2	29	18	21	80	70	90	50	20	41	47	35
Semiquantitative emission spectrography													
Ag	N0.5	N0.5	N0.5	N0.5	N0.5	N0.5	N0.5	N.5	N0.5	N0.5	N0.5	N0.5	N0.5
Ba	30	30	<20	20	30	100	70	100	30	50	50	100	1,000
Co	N10	100	300	30	70	70	200	200	30	70	70	70	30
Cr	150	150	200	300	700	700	1,000	3,000	150	700	1,000	1,000	100
Cu	30	20	50	30	70	100	150	150	50	50	50	50	100
Mn	200	700	1,500	1,000	700	1,000	1,500	1,500	700	1500	2,000	2,000	200
Ni	15	10	150	150	150	300	700	1,000	100	100	150	150	100
Pb	<10	N10	<10	<10	15	<10	<10	<10	<10	<10	10	10	10
V	70	50	70	100	150	150	150	200	100	150	200	200	100

[1]Contains 20 ppm Mo.
[2]Contains 5 ppm Mo.
[3]Contains 10 ppm Mo.

	UV–62–89	UV–63–89	UV–64–89	UV–65–89	UV–66–89	UV–67–89	UV–81–89	UV–82–89	UV–83–89	UV–84–89	UV–85–89	UV–86–89	UV–87–89
Gold and trace elements by various methods													
Au	<2	<2	<2	<2	<2	<2	<2	<2	<2	4	<2	<2	<2
As	<5	<5	17	5	151	11	375	39	29	427	13	<5	46
Cd	0.1	0.3	0.8	<0.1	0.4	<0.1	0.4	<0.1	<0.1	0.3	<0.1	<0.1	<0.1
Hg	0.02	N0.02	0.04	N0.02	N0.02	N0.02	N0.02	N0.02	N0.02	N0.02	N0.02	N0.02	N0.02
Sb	<2	<2	<2	<2	<2	<2	<2	<2	<2	5	<2	<2	<2
Se	<0.2	<0.2	0.6	0.3	0.3	<0.2	0.9	<0.2	<0.2	1.0	<0.2	<0.2	0.3
Tl	0.20	0.25	0.30	<0.05	<0.5	<0.05	0.25	<0.05	<0.05	<0.05	<0.05	<0.05	<0.05
Ti	<0.05	<0.05	<0.05	<0.05	<0.05	<0.05	<0.05	<0.05	<0.05	<0.05	<0.05	<0.05	<0.05
Zn	5	14	22	6	27	<2	9	2	3	15	2	<2	5
Semiquantitative emission spectrography													
Ag	N0.5	N0.5	N0.5	N0.5	N0.5	N0.5	N0.5	N0.5	N0.5	N0.5	N0.5	N0.5	N0.5
Ba	300	50	300	100	200	30	20	20	30	100	30	50	20
Co	15	20	70	200	100	N10	10	N10	N10	70	N10	N10	20
Cr	150	200	300	70	2,000	20	500	200	150	700	50	10	200
Cu	30	30	200	70	100	5	70	30	15	50	30	7	50
Mn	700	700	3,000	3,000	1,500	700	300	150	500	1,500	150	20	700
Ni	70	100	150	100	500	5	100	30	15	300	20	5	70
Pb	<10	<10	15	N10	10	N10	10	<10	<10	<10	N10	N10	N10
V	150	150	200	30	150	20	150	70	50	150	30	<10	70

	UV–88–89	UV–89–89	UV–91–89	UV–92–89	UV–93–89	UV–94–89	UV–95–89	UV–96–89	UV–97–89	UV–98–89	UV–99–89	UV–100–89
Gold and trace elements by various methods												
Au	2	650	2	2	18	4	2	<2	<2	10	N2	N2
As	64	695	138	235	50	33	47	79	110	48	9	<5
Cd	<0.1	0.9	<0.1	<0.1	<0.1	<0.1	<0.1	<0.1	<0.1	<0.1	<0.1	<0.1
Hg	N0.02	N0.02	N0.02	N0.02	N0.02	N0.02	0.04	N0.02	N0.02	N0.02	N0.02	N0.02
Sb	<2	6	<2	2	<2	<2	5	4	3	<2	<2	<2
Se	0.3	1.1	1.1	0.5	<0.2	<0.2	0.3	0.3	0.3	0.3	0.3	<0.2
Tl	<0.05	0.40	0.35	0.65	<0.05	<0.05	N0.05	N0.05	N0.05	N0.05	N0.05	N0.05
Ti	<0.05	<0.05	<0.05	<0.05	<0.05	<0.05	N0.05	N0.05	N0.05	N0.05	N0.05	N0.05
Zn	3	32	4	7	<2	<2	4	4	4	<2	4	<2
Semiquantitative emission spectrography												
Ag	N0.5	N0.5	N0.5	N0.5	N0.5	N0.5	--	--	--	--	--	--
Ba	20	30	30	30	20	30	--	--	--	--	--	--
Co	<10	30	<10	15	N10	N10	--	--	--	--	--	--
Cr	150	700	200	200	100	150	--	--	--	--	--	--
Cu	30	300	50	70	30	20	--	--	--	--	--	--
Mn	150	300	30	70	50	50	--	--	--	--	--	--
Ni	50	200	50	100	15	20	--	--	--	--	--	--
Pb	N10	15	N10	<10	N10	N10	--	--	--	--	--	--
V	70	100	70	70	30	50	--	--	--	--	--	--

Table 2. Gold and trace-element analyses of rock and soil samples from quartz veins in the Pistón de Uroy area, Venezuela—Continued.

Sample descriptions					
V1	Chip sample of quartz vein	UV–10–89	Chip sample of oxide-rich quartz, 1 m thick	UV–37–89	Chip sample of altered, weathered rock
V2	Chip sample of quartz vein	UV–11–89	Chip sample of altered, oxide rich quartz vein, 1 m thick	UV–38–89	Chip sample of altered rock, 30 cm thick
V3	Chip sample of quartz vein	UV–12–89	Chip sample of white quartz with limonite, 3 m thick	UV–39–89	Chip sample from block of oxide altered quartz vein
V4	Chip sample of quartz vein	UV–13–89	Chip sample of foliated quartz blocks	UV–42–89	Grab sample of gray quartz with visible sulfide minerals
V5	Chip sample of quartz vein	UV–14–89	Yellow soil, channel sample across 25-cm interval	UV–43–89	Grab sample of vuggy quartz with terminated quartz crystals
V6	Chip sample of quartz vein	UV–15–89	Red-brown soil, channel sample across 50-cm interval	UV–45–89	Grab sample of oxide-rich quartz vein
V7	Chip sample of quartz vein	UV–16–89	Yellow soil, channel sample across 30-cm interval	UV–46–89	Grab sample of altered pyroxenite, vein country rock
V8	Chip sample of quartz vein	UV–17–89	Red-brown soil, channel sample across 35-cm interval	UV–47–89	Grab sample of oxide-rich quartz vein
V9	Chip sample of quartz vein	UV–18–89	Oxidized quartz vein, channel sample across 40-cm interval	UV–48–89	Grab sample of quartz-vein float
V10	Chip sample of quartz vein	UV–19–89	Red-brown soil, channel sample across 40-cm interval	UV–49–89	Grab sample of quartz vein
V11A	Chip sample of quartz vein	UV–20–89	Yellow soil, channel sample across 20-cm interval	UV–50–89	Grab sample of gray quartz vein
V11B	Chip sample of quartz vein	UV–21–89	Red-brown soil, channel sample across 40-cm interval	UV–51–89	Chip sample of quartz vein and altered rock, 1 m thick
V12	Chip sample of quartz vein	UV–22–89	Red-brown soil, channel sample across 20-cm interval	UV–52–89	Chip sample of quartz vein and altered rock, 1 m thick
V13	Chip sample of quartz vein	UV–23–89	Red-brown soil, channel sample across 135-cm interval	UV–53–89	Chip sample of quartz vein and altered rock, 2.5 m thick
V14	Chip sample of quartz vein	UV–24–89	Red-brown soil, channel sample across 30-cm interval	UV–54–89	Quartz stockwork in altered rock, 20 cm thick
V15	Chip sample of quartz vein	UV–25–89	Red-brown soil, channel sample across 150-cm interval	UV–55–89	Quartz veinlets in altered rock, 20 cm thick
V16	Chip sample of quartz vein	UV–26–89	Red-brown soil, channel sample across 150-cm interval	UV–56–89	Chip sample of quartz vein, 20 cm thick
V17	Chip sample of quartz vein	UV–27–89	Chip sample from blocks of quartz vein	UV–57–89	Chip sample of altered rock, 70 cm thick
UV–1–89	Chip sample of white quartz vein, approximately 5 m thick	UV–28–89	Chip sample from altered quartz-carbonate boxwork, about 5 m thick	UV–58–89	Chip sample of quartz vein and altered rock, 1.5 m thick
UV–2–89	Chip sample of oxide material and quartz from blocks	UV–29–89	Chip sample from quartz-carbonate boxwork, 1 m thick	UV–59–89	Chip sample of quartz vein and altered rock, 1.5 m thick
UV–3–89	Chip sample of white quartz, 0.5 m thick	UV–30–89	Chip sample from altered ultramafic rock, 50 cm thick	UV–60–89	Chip sample of quartz vein and altered rock, 1.5 m thick
UV–4–89	Chip sample of gray brecciated quartz, 2.5 m thick	UV–31–89	Quartz-carbonate vein, 2 cm thick	UV–61–89	Grab sample fragmental, altered volcanic rock
UV–5–89	Chip sample of foliated white quartz, 2 cm thick	UV–32–89	Chip sample of altered rock, 50 cm thick	UV–62–89	Chip sample of quartz vein, 1 m thick
UV–6–89	Chip sample of altered, foliated quartz, 30 cm thick	UV–33–89	Quartz-carbonate vein, 2 cm thick	UV–63–89	Chip sample of quartz vein, 1 m thick
UV–7–89	Chip sample of altered ultramafic rock, 2 m thick	UV–34–89	Chip sample of altered rock, 120 cm thick	UV–64–89	Chip sample from blocks of quartz vein
UV–8–89	Chip sample of foliated oxide quartz, 1 m thick	UV–35–89	Quartz-carbonate vein, 2 cm thick	UV–65–89	Grab sample oxide-rich quartz vein
UV–9–89	Chip sample of white quartz, 50 cm thick	UV–36–89	Chip sample of altered rock, 47 cm thick	UV–66–89	Chip sample from block of quartz vein

UV–67–89	Chip sample from block of quartz vein and altered pyroxenite	UV–87–89	Massive white quartz from same block as UV–86–89	UV–94–89	Vuggy quartz from same block as UV–86–89	
UV–81–89	Massive white quartz from block	UV–88–89	Vuggy quartz from same block as UV–86–89	UV–95–89	Oxide–rich vuggy quartz from same block as UV–86–89	
UV–82–89	Oxide-rich material in same block as UV–81–89	UV–89–89	Massive white quartz from same block as UV–81–89	UV–96–89	Oxide–rich vuggy quartz from same block as UV–86–89	
UV–83–89	Finely brecciated quartz with hematite filled fractures	UV–91–89	Vuggy quartz, oxide filling fractures from same block as UV–86–89	UV–97–89	Milky quartz with vugs filled with oxides from same block as UV–81–89	
UV–84–89	Coarsely brecciated quartz from same block as UV–81–89	UV–92–89	Vuggy quartz, oxide filling fractures from same block as UV–86–89	UV–98–89	Milky quartz with vugs filled with oxides from same block as UV–86–89	
UV–85–89	Massive white quartz from same block as UV–81–89	UV–93–89	Massive white quartz, from same block as UV–86–89	UV–99–89	Brecciated quartz with oxide filled fractures from same block as UV–86–89	
UV–86–89	Vuggy brecciated quartz from block					

The trace-element content of the rocks is typical of that of ultramafic and mafic rocks. The copper content (table 1) correlates with the amount of chalcopyrite in polished sections and thus reflects well the amount of sulfide minerals in the rocks (table 2). The chromium content in the ultramafic rocks represents the amount of chromite. Some of the rock samples (UGP–5, UGP–17, UGP–38, UGP–39) contain anomalous amounts of platinum-group elements. Although a platinum-group mineral was not identified in the polished sections, sperrylite ($PtAs_2$) was identified in scanning electron microscope images (see fig. 3). Chondrite-normalized diagrams for the platinum-group elements show that cumulates containing cumulus chromite have a different type of pattern than those for the other types of cumulates, which show positive slopes reflecting the concentration of platinum-group elements by a process associated with sulfide mineral formation (fig. 4). The saw-toothed chondrite-normalized pattern for rocks that contain cumulus chromite may be the result of iridium, ruthenium, and rhodium concentration at the time of chromite precipitation and platinum and palladium concentration at the time of sulfide formation.

Samples UGP–5, UGP–17, UGP–38, and UGP–39 have the highest platinum-group element values and were examined for platinum-group minerals using the scanning electron microscope. Platinum-group minerals were not found in samples UGP–5 and UGP–17. Sample UGP–39 contained a grain of platinum and arsenic enclosed in a composite grain of chalcopyrite (fig. 3). The extremely small size of the grain precluded quantitative analysis; however, the qualitative data suggest that the mineral is sperrylite ($PtAs_2$). Sample UGP–38 also contained sperrylite, as well as a (Pt, Te, Ni, As) mineral (possibly moncheite), a (Pt, Fe, Ir) alloy, and a (Pt, Ir, Rh, As, S) mineral (possibly hollingworthite).

Gold in vein material and soil samples ranges from less than 2 to 4,640 ppb; the arithmetic mean of unqualified values is 292.6 ppb, and the geometric mean is 33.1 ppb (table 2). Arithmetic and geometric means and standard deviation for the number of unqualified values for the analyses of vein material from table 2 are listed in table 3. Large differences between the arithmetic and geometric means and the relatively large standard deviations indicate the skewed nature of the normal distributions for most elements. Significant one-to-one correlations of lognormalized data exist between Mn, Co, Cr, Cu, and Ni; Cr, Mn, and Ni; Ni and Zn; As, Ni and Se; Se and Tl; Tl and Hg; Ba, Co, and Cu; and Au and Cd. The correlation with manganese reflects the development of manganese-iron oxide minerals and the absorption of other elements such as copper during weathering. The associations of arsenic, selenium, and tellurium probably reflect introduced materials related to mineralization.

In order to ascertain relations between metallic elements and elements other than gold, the data set in table 2

Table 3. Statistical parameters for unqualified values of analyses of quartz-vein material given in table 2.
[In parts per million except for gold, which is in parts per billion]

	Mean	Standard deviation	Geometric mean	Number of unqualified values
Au	292.6	793.6	33.1	69
As	103.8	189.8	35.5	93
Cd	0.83	0.58	0.63	47
Hg	0.08	0.26	0.03	42
Sb	4.1	1.5	3.8	14
Se	0.65	0.76	0.48	62
Te	0.19	0.21	0.14	46
Tl	0.18	0.17	0.13	37
Zn	37.1	39.7	19.2	75
Ag	3.8	3.7	2.0	4
Ba	188.0	548.2	75.4	88
Co	109.9	146.7	66.2	74
Cr	598.0	805.2	260.5	98
Cu	134.7	178.9	70.9	96
Mn	1,683.4	1,262.5	547.6	98
Ni	205.0	292.6	89.5	95
Pb	13.6	2.8	13.3	36
V	104.0	55.9	85.3	96

was split into sets of groups. In one split, samples containing less than 2 ppb Au were separated from samples having unqualified values. Mean values for arsenic, copper, and zinc of these two sample groups are different at a 99 percent confidence level, and mean values for cadmium, chromium, mercury, and nickel are different at a 95 percent confidence level. In another split, samples whose gold content is above the mode of gold contents and below the mode were tested; only the means for cadmium, zinc, and copper showed significant differences between the two groups of samples. The significant differences in means of elements of the sample groups split on gold content may indicate that these elements were introduced to the vein system during mineralization. Copper and zinc probably are the best pathfinder elements for rocks that contain gold.

GEOPHYSICS

Soil and jungle cover is extensive in the Pistón de Uroy area, and several geophysical methods were used in order to obtain information on the buried rocks that host the quartz-vein system. Surveys were made using magnetic, induced polarization, and very low frequency electromagnetic methods. In addition, a group of students from Universidad de Simon Bolívar (Caracas) conducted a gravity survey at Pistón de Uroy (V.R. Graterol, written commun., 1989), but the data are not usable because local topography is steep, and topographic data were not collected for topographic corrections.

Following the initial geologic mapping, a grid was carefully surveyed and marked in anticipation of the geophysical surveys (plate 1). This grid is subsequently referred to as the geophysical grid to distinguish it from the original geologic (reconnaissance) grid (fig. 2). Traverse lines, called picas, were spaced 200 m apart along the 4-km-long baseline, called the eje. The eje is oriented N. 80° E., and the picas are oriented perpendicular to the eje. In part because the topography is more rugged near the scarp of the Roraima Group to the north, all of the northern part of the quartz-vein system discovered during the geological mapping (see fig. 2) was not adequately sampled using the geophysical methods.

DATA ACQUISITION, PROCESSING, AND ANALYSIS

MAGNETIC DATA

Total-field magnetic data were acquired in January and May 1989 at 20-m intervals along both the geological and geophysical grids using Geometrics model 816 and Scintrex model MP–2 magnetometers. A base station magnetometer was unavailable, but base stations were remeasured, on average, every one or two hours. The data were given UTM coordinates and reduced for drift (diurnal) correction using a computer program called SPDM3 (Alí Fernández, Corporación Venezolana de Guayana, Técnica Minera, C.A., written commun., 1989) and were gridded and plotted using a commercial software package called GDM developed by the Bureau de Recherches Géologique et Minières (fig. 5). The contoured data show a distinctive linear anomaly in the northern part of the geophysical grid caused by a strongly magnetic body trending roughly N. 75° E. This anomaly correlates closely with peridotite outcrops and may be caused by the ultramafic body mapped by Page and Contreras (written commun. from Norman J Page, U.S. Geological Survey, and Gloria Contreras, Técnica Minera, C.A., March 9, 1988, to Vicente Mendoza and César Gutiérrez, Técnica Minera, C.A., and February 16, 1989, to Vicente Mendoza, Fernando Susach, and Nestor Angulo, Técnica Minera, C.A.) (see also Contreras and Freites, 1989). The anomaly suggests that a larger continuous peridotite body is present in the subsurface.

A series of two-dimensional models was calculated along the picas using the MAGMOD3 software by Geosoft in an attempt to outline the surface trace of the peridotite body. This modeling is particularly important because the inclination of the Earth's magnetic field at Pistón de Uroy of about 31° leads to strong distortion and to lateral shifts of the anomalies from their source rocks. Figure 6 shows the magnetic data with the modeled causative body from pica 11, approximately in the middle of the geophysical grid. When

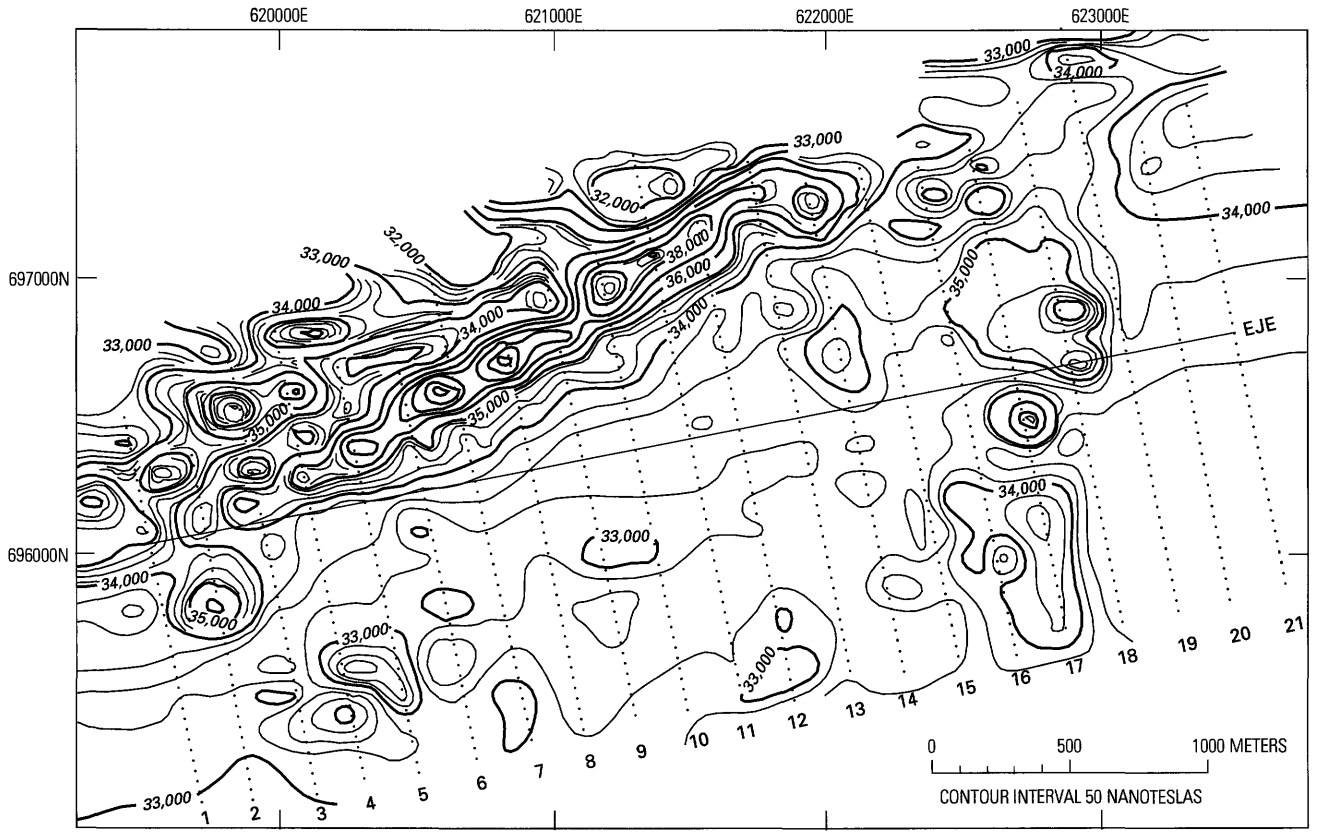

Figure 5. Total-field magnetic map for the Pistón de Uroy area, Venezuela. Geophysical grid is shown in figure 2. Contour interval 50 nanoteslas (nT); dots show station locations along picas (traverse lines).

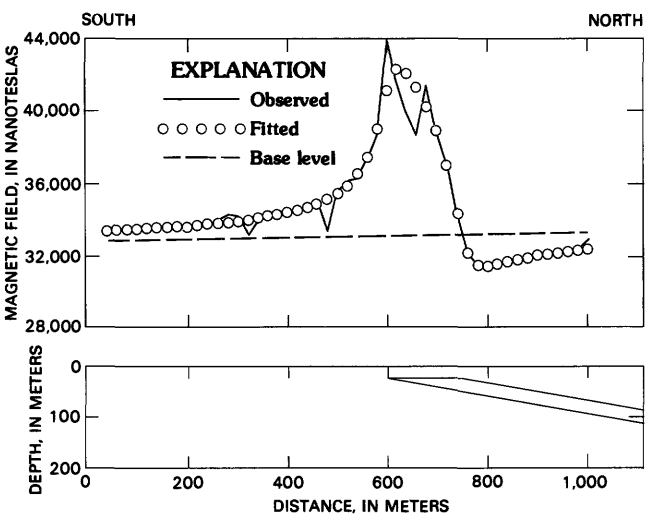

Figure 6. Magnetic model profile showing inferred causative body, pica 11 of geophysical grid shown in figure 2, Pistón de Uroy area, Venezuela. The best susceptibility fit uses a long, narrow body that is buried 24 m below the surface, dips 10° N., and has a half-width of 72 m. The modeled susceptibility is 0.358 emu. The Earth's field strength is taken to be 32,700 nT, field inclination 31°, and declination −11°. See text for discussion.

the model results were combined, it was possible to infer, in map view, the location, size, and dip of the peridotite body.

VERY LOW FREQUENCY ELECTROMAGNETIC DATA

Recognition of offsets and truncations of the quartz veins early in the geological mapping phase (Norman J Page and Gloria Contreras, written commun., March 9, 1988, to Vicente Mendoza and César Gutiérrez) led to speculation about a late-stage series of offsetting faults, apparently striking north. In an attempt to correlate probable offsets in two parts of the quartz-vein system, very low frequency electromagnetic measurements were made. Because the transmitting station was oriented almost due north, only the positive crossovers (that is, where dip angles of the very low frequency electromagnetic field are positive to the left, negative to the right) indicate the presence of a conductor (for instance, a water- and gouge-filled fault or narrow shear zone) at the midpoint (see fig. 7). The very low frequency electromagnetic method allows rapid reconnaissance (data can be acquired at almost the speed at which one can walk), but it is relatively limited in depth penetration (about 60–100 m in resistivities such as those encountered at Pistón de

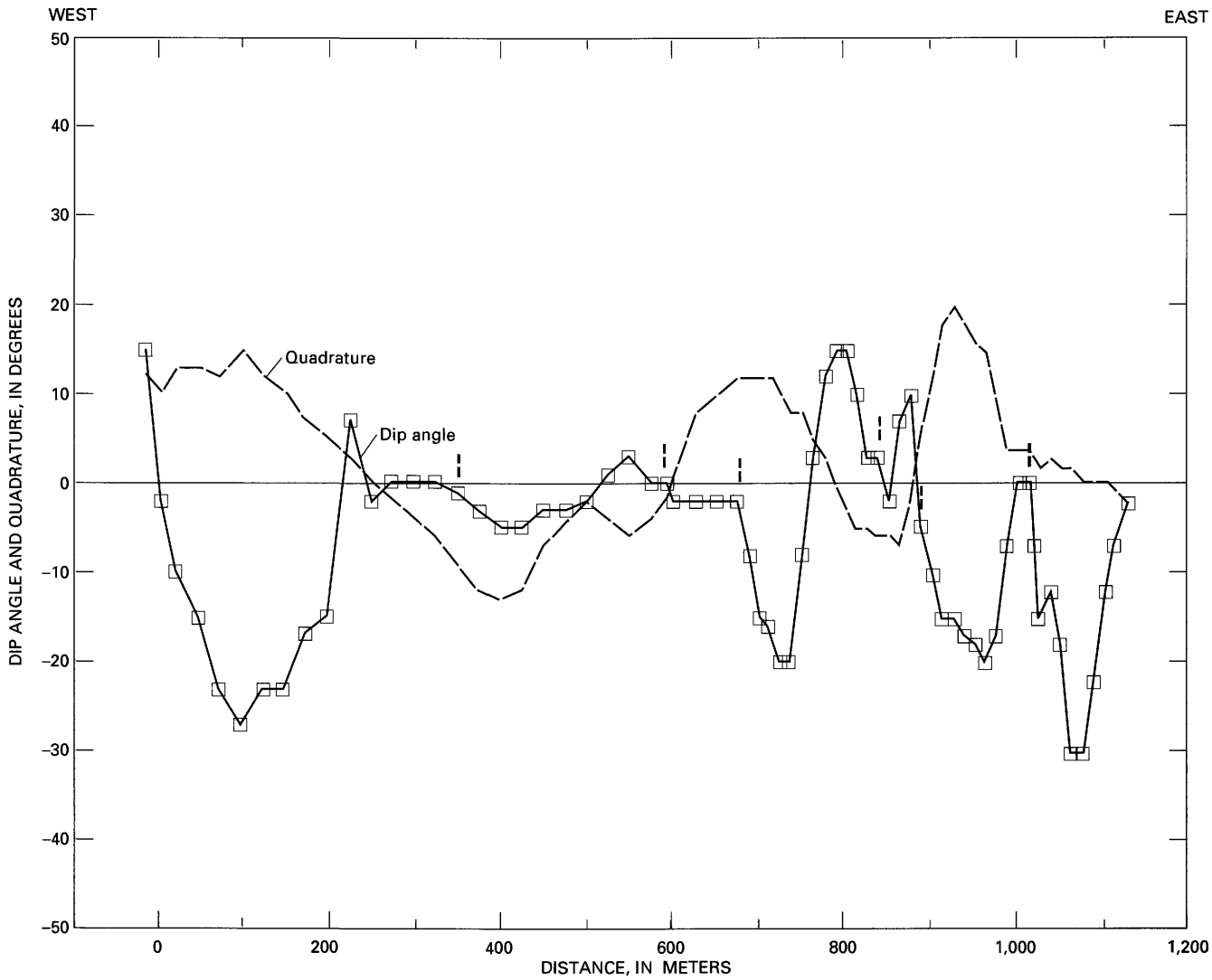

Figure 7. Very low frequency electromagnetic profile along the baseline (eje) of the geologic grid shown in figure 2, Pistón de Uroy area, Venezuela. The vertical dashed bars indicate probable water-filled faults that offset the quartz-vein system.

Uroy). The depth of penetration depends on the resistivity of the uppermost materials being measured.

Very low frequency electromagnetic data were acquired in January 1989 using a Geonics EM–16 system and were plotted (fig. 7) using conventions discussed in Fraser (1969). An insufficient number of parallel profiles were acquired to justify a derivative filter approach (Fraser, 1969). Two profiles were made, one along the geologic baseline or eje (fig. 2) and one parallel with it but 100 m to the north. Correlation of crossovers between these two parallel lines supports the possibility that a series of faults striking about N. 10° W. offsets the quartz-vein system in several places (shown by the vertical bars in fig. 7). In addition, large (as much as 30°) dip angles at 00 m and 1,000 m suggest that two major conductors (large, water-filled fault zones) are coincident with the La Franela and El Pistón stream channels (fig. 2).

INDUCED POLARIZATION DATA

Since World War II, the induced polarization (IP) method has been used successfully to detect disseminated sulfide minerals in rocks (Sumner, 1976). During the 1970's, it was determined that the induced polarization method could be used as a mapping tool by outlining systematic variations in clay and metallic sulfide mineral contents (Zonge and Wynn, 1975). In some cases, the induced polarization method can detect the presence of pyrite in amounts of less than 0.1 percent and thus is an ideal tool to assist in separating otherwise indistinguishable lithologies. The induced polarization effect is caused by frequency-dependent variations in resistivity; consequently, resistivity data are obtained during induced polarization measurements as additional information. Variations in resistivity normally correlate closely with porosity, at least in the absence of

heterogeneities such as clay layers or metallic sulfide minerals. The more water present (for example, in a fault zone), the lower the apparent resistivity. Induced polarization data were collected in the Pistón de Uroy area to assist in mapping hidden fault zones and to delineate the buried rock units that may have controlled emplacement of the quartz veins.

Time-domain induced polarization data were collected over most of the geophysical grid in May 1989 using the gradient array configuration (Sumner, 1976; Alí Fernández, written commun., 1989) and a Scintrex TSQ series transmitter and IPR–10A time-domain receiver. A transmitter dipole 3,000 m long was set up along a pica, and smaller receiver dipoles were used both inline—that is, along the same pica, but only inside the center 2,000-m zone of the transmitter—and as many as two picas (400 m) away offline. Both 40-m and 80-m receiver dipole lengths were used, and receiver dipoles were moved 20 m between measurements. The 40-m receiver dipole data are not shown here because they are incomplete due to noise; commonly, the field operators did not record the values because the receiver would not stabilize. The 80-m data were given UTM coordinates and reduced to apparent resistivity values using a computer program called POLARIN (Alí Fernández, written commun., 1989). They were smoothed using a five-point low-pass filter and plotted using Lotus Symphony (for profiles) and SURFER4 (for plan maps).

Figure 8 represents a plan view of the resistivity data for 80-m dipoles acquired along the picas of the geophysical grid in the Pistón de Uroy area. The data show four anomalous (resistive) zones in a host-rock resistivity background of about 1,000 ohm-m.

In the western half of the map area (fig. 8), north of the eje, a high-resistivity (as much as 4,000 ohm-m) linear anomaly strikes about N. 80° E. and probably coincides with the eastern part of the western quartz-vein system. Mapping of the quartz-vein system in this area shows true widths of as much as 5 m. The resistive anomaly is truncated toward the east at about pica 11, in exactly the same manner as the mapped quartz vein, and probably extends westward at least as far as pica 2. This coincidence is remarkable for two reasons: one, it implies that the quartz-vein system has sufficient volume to be recognizable even with dilution of the resistivity by the surrounding rock, and, two, it signifies that the vein may extend at least 700–800 m farther to the west than is shown by surface mapping. This latter observation also implies that the vein is subparallel with, but eventually cuts, the peridotite body at an oblique angle, a relation that makes the quartz-vein system one of the youngest geological features in the area.

The unusual size or volume of the vein system contributes to its potentially economic importance. Note that with an 80-m receiver dipole, the induced polarization system is sampling and averaging over a roughly hemispherical volume of rock centered around the dipole. Dilution of the resistivity by the surrounding rocks and soils to the resistivity contribution of a 2–5-m-wide quartz vein should therefore be substantial. Initially, it was expected that the induced polarization data would help in mapping rock types. A weak induced polarization anomaly over this part of the quartz-vein system is remarkable, which suggests that the total volume of the quartz-vein system is large.

Just south of the linear, so-called quartz-vein anomaly shown in figure 8 is a strong, discrete anomaly that is only expressed on picas 8 and 9. Resistivity values are greater than 9,000 ohm-m. The source body strikes N. 40° E. and is as wide as 200 m and at least as long as 350 m. The exact nature of the source is not clear, but it may be related to a gabbro inferred to be present from isolated float in the area of the anomaly. The source body may connect with another body to the east.

The third resistivity anomaly is an apparent eastern extension of the second. A profile across it is discussed following. In one place (pica 14), resistivity of more than 20,000 ohm-m suggests a dense, extremely low porosity, possibly silica-flooded rock. Although it is possible that current leakage caused this high apparent resistivity, it is unlikely because the high resistivity is coherent across several picas.

A fourth resistivity anomaly of as much as 9,000 ohm-m is parallel with the third anomaly but farther to the south. Comparison of the 40- and 80-m receiver dipole data for this southeastern anomaly suggests that the source body may dip south-southeast. This interpretation is not as certain as the dip (calculated from magnetic models) of the peridotite body farther to the north, which dips north.

Figure 9 represents a plan view of the chargeability data from the induced polarization survey. Though filtered by the contouring package, the substantial amplitude of the noise nevertheless is evident; the noise is even greater in the 40-m receiver dipole data. Two or three anomalies are clearly visible in figure 9. The westernmost anomaly is south of the eje, completely on pica 7, and probably is unrelated to the resistivity anomaly on picas 8 and 9. This anomaly has characteristics that suggest it is cultural in origin. Although a geologic origin cannot be completely excluded, the anomaly probably reflects buried debris left by miners working in the area.

The second most obvious chargeability anomaly shown in figure 9 is a linear feature about 100 m wide along profile, parallel with and about 150 m north of the eje, starting about pica 9 and extending at least 700 m through pica 12. Chargeabilities are as high as 60 msec on pica 10 and as high as 50 msec on pica 12 (see below). These relatively high values are probably due to disseminated pyrite (or possibly ilmenite), probably at least 2–3 percent by volume. This anomaly is close to, but not coincident with, the resistivity anomaly that is correlated with the western quartz-vein system. The area of the anomaly is a primary drill target.

Figure 10 shows a resistivity and chargeability profile along pica 12; these data are for an 80-m receiver dipole length. The chargeability data are relatively noisy, primarily

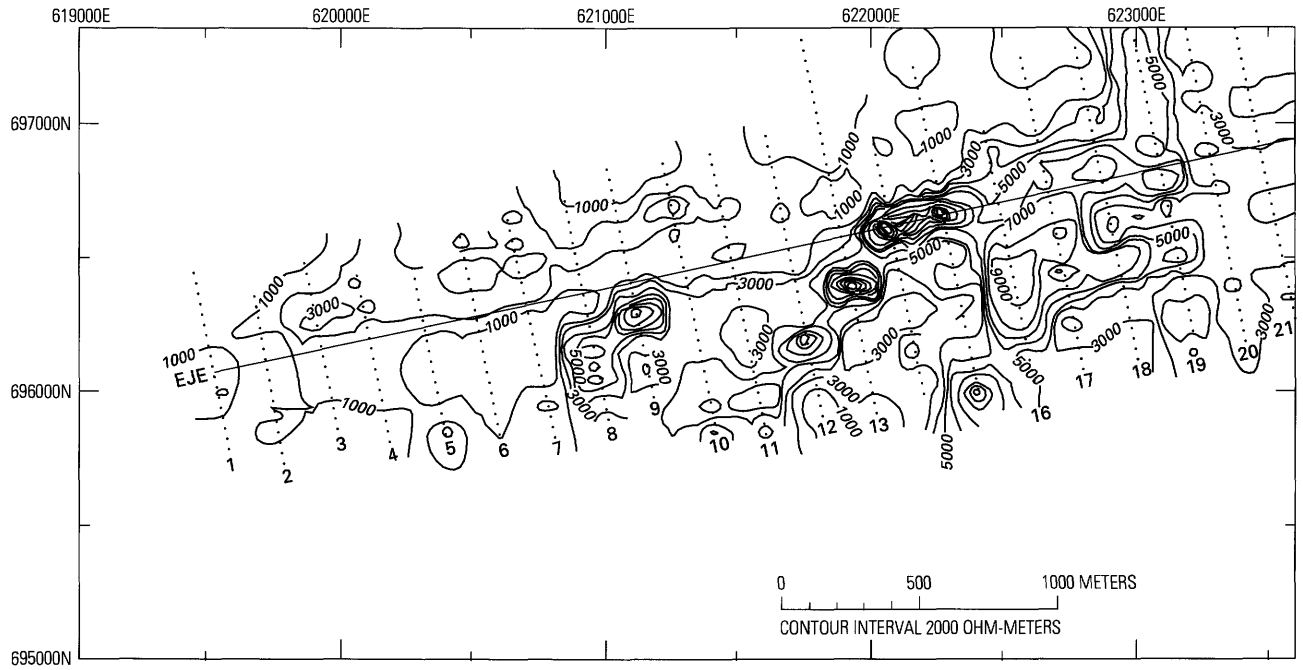

Figure 8. Map showing contours of gradient-array resistivity data (3,000-m transmitter dipole and 80-m receiver dipole) from the induced polarization survey acquired on the geophysical grid shown in figure 2, Pistón de Uroy area, Venezuela. This array is analogous to AB=3,000 m and MN=80 m in Schlumberger array resistivity surveys for the limiting case of the receiver dipole inline and centered in the middle of the transmitter dipole. Contour interval 2,000 ohm-m. Dots indicate station locations along picas (traverse lines).

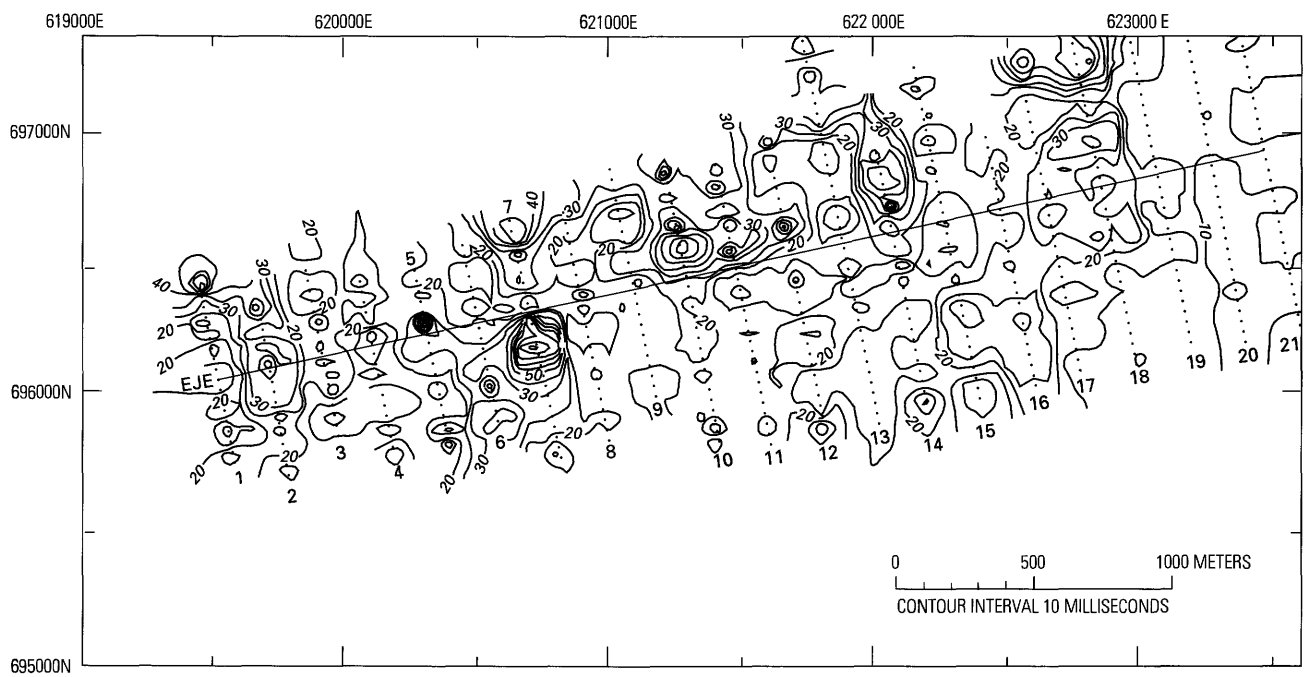

Figure 9. Map showing contours of chargeability data (polarization component) from the same induced polarization survey shown in figure 8. Contour interval 10 msec.

because the field operators did not average sufficient readings at each station. The 40-m receiver dipole chargeability data along this same profile, although providing better resolution, are in general too noisy to use except to roughly estimate dip direction of the polarized bodies at depth. A five-point digital filter (fig. 10, solid line) was applied to the 80-m chargeability data in order to distinguish between rock types along the profile. The resistivity profile (fig. 10)

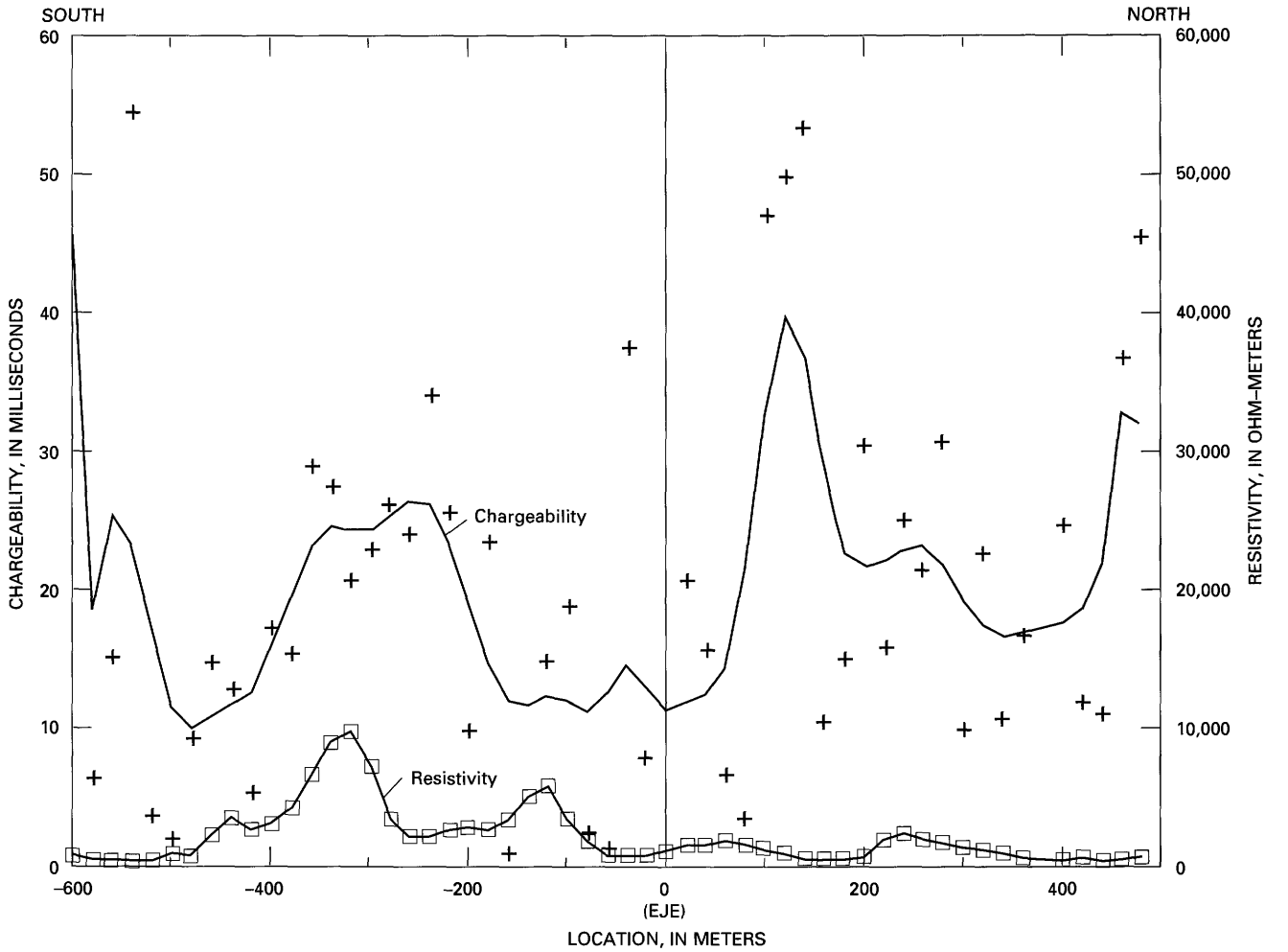

Figure 10. Resistivity (squares) and chargeability (pluses) profiles along pica 12 of the geophysical grid shown in figure 2, Pistón de Uroy area, Venezuela. Data were acquired using an 80-m receiver dipole spacing. Pluses represent original, noisy chargeability data, whereas the smooth curve represents a five-point (weighted) filtered version.

shows two distinct resistivity highs that probably represent silica-flooded (and therefore lower porosity) rocks. The southern high, centered about stations –300 and –400, can be traced from profile to profile, and probably represents a distinct lithostratigraphic unit. The apparent resistivity of the unit is greater than 10,000 ohm-m, a value that could reflect a true inherent resistivity as high as 30,000–50,000 ohm-m. The southern high is associated with a significant chargeability anomaly of as much as 35 msec. The apparent resistivity and chargeability anomalies together indicate a 100–150-m-wide unit containing perhaps 2 percent pyrite and having much lower porosity (late-stage silica flooding or a relatively nontectonized intrusive rock) than the surrounding (volcanic?) rocks. The second resistivity high, around station –140, is similar to the first but is lower in amplitude, both in resistivity and in chargeability. It probably represents similar rock but a narrower width.

On the north side of the eje, centered around station 120 (figs. 9, 10), is a chargeability anomaly; the resistivity is at or less than the background average of 1,000 ohm-m. The anomaly is significant: three stations in sequence have chargeabilities of about 50 msec. The anomaly extends from pica 12 west to pica 9 and cannot be dismissed as mining debris. It is probably caused by a discrete geologic unit, only 50–100 m wide, containing several percent by volume of either clay (for instance, montmorillonite) or possibly sulfide minerals or ilmenite (but probably pyrite). It is significant that this anomaly is subparallel with the western quartz-vein system but extends several hundred meters beyond it to the east. The anomaly may represent a completely hidden mineralized body.

INTEGRATION OF THE GEOPHYSICAL DATA

Figure 11 combines the known (mapped) expressions of the quartz-vein system and an interpretation of the three geophysical data sets. The western quartz-vein system may

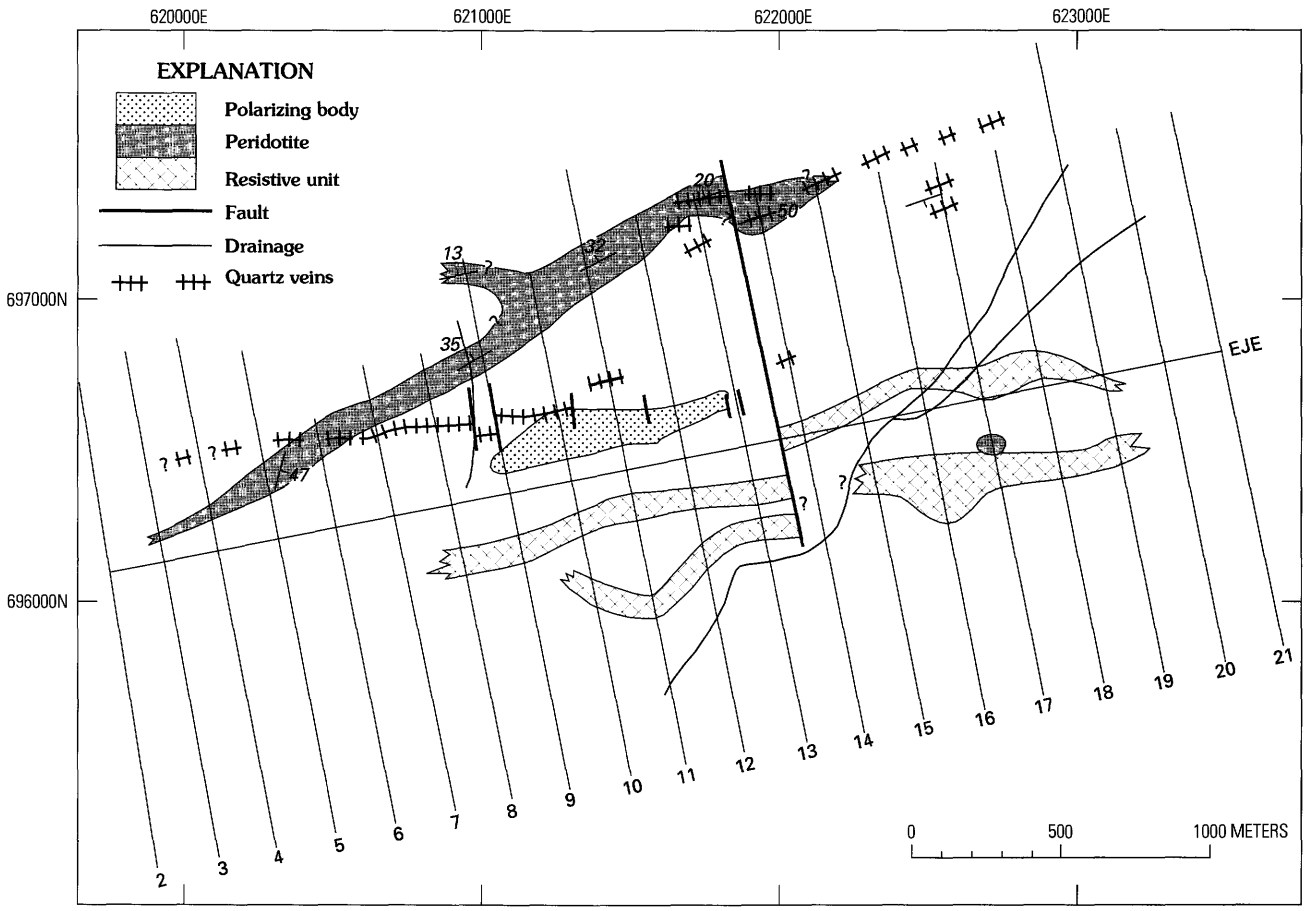

Figure 11. Map showing interpretation of magnetic, very low frequency electromagnetic, and induced polarization data and results of geological mapping of the quartz-vein system, Pistón de Uroy area, Venezuela. Geophysical grid is shown in figure 2.

extend 700–800 m farther to the west than mapped; however, it may or may not be offset 600 m by a left-lateral fault that is roughly parallel with, and between, picas 11 and 12. In fact, the western quartz-vein system may be a separate entity. Nevertheless, a N. 10° W.-striking conductor, probably a fault, is present at this point. Although the very low frequency electromagnetic data and field mapping show several short north-south offsets along the western vein system, the presence of a large-displacement transcurrent fault between picas 11 and 12 is belied by the relative continuity of two different (roughly east trending) bodies mapped by the induced polarization survey and by the relatively continuous peridotite body inferred from the magnetic data. It is likely, therefore, that the eastern vein system has always been separate from the western vein system.

The peridotite body on the north edge of the geophysical grid trends east-northeast, dips north for most of its length, and is more extensive in the subsurface. Magnetic susceptibility values for the peridotite (in outcrop) are about ten times those of the surrounding gabbro.

The highly polarized unit just north of the geophysical eje, between picas 9 and 12, is an enigma. It probably has a significant sulfide content and is subparallel with, and apparently related to, the eastern part of the western quartz-vein system.

The two parallel resistive units on and south of the geophysical eje in the central and eastern parts of the Pistón de Uroy area probably represent rocks that contain small amounts of sulfide minerals and have low porosity. This low porosity could be caused by silica flooding or by metamorphism; the source body could be a relatively dense volcanic rock without subsequent fractures due to tectonism. Although comparison of the 40-m and 80-m dipole data suggests some south-with-depth displacement of these resistive bodies, the strong noise in these data makes that interpretation far from certain.

CONCLUSIONS

In the Pistón de Uroy area of Estado Bolívar, Venezuela, a quartz-vein system is subparallel with the strike of, and is hosted by, an ultramafic body. The cumulate ultramafic rocks and gabbro intrude an older greenstone belt that contains volcanic rocks of andesitic to basaltic character. Unconformably overlying these rocks is the basal section of

sandstone and quartz-pebble conglomerate of the Early Proterozoic Roraima Group.

The gold-bearing quartz-vein system in the Pistón de Uroy area is roughly along the geologic baseline and north of the geophysical baseline. Although it appears that two segments of a single quartz-vein system are offset 600 m in a left-lateral direction, the continuity of adjacent subparallel units indicates that the eastern and western veins are probably distinct from each other. The quartz veins are unusually wide, 8 m or more at one location on the eastern vein, and, by virtue of their significant effect on the electrical resistivity data, they must constitute a large volume of rock. The overall length of both systems, including a probable 700–800 m extension of the western vein as suggested by the geophysical data, is at least 3,000 m. Gold values are as high as 4,640 ppb in the western vein system and as high as 220 ppb in the eastern vein system.

Both geologic mapping and geophysical data suggest that at least two sets of faults are present in the area. One set cuts the quartz-vein system and strikes approximately N. 10° W., probably postdating the quartz veins, and has offsets typically less than 100 m. The other set probably is part of a regional series of major shear zones that possibly follow older Precambrian structures. The shear zones are younger than the quartz veins because they are now highly conductive (water filled) and have not been recemented during metamorphism. The quartz-vein system has not been identified east of the El Pistón stream drainage. If the shear-zone system has had any significant movement since emplacement of the quartz veins at Pistón de Uroy, then movement has been greater than 1 km, which is the size of the vein-free ground examined east of the shear zone. This is unlikely.

Geophysical data suggest the presence of additional lithologic units not mapped on the surface. A hidden, strongly polarizing body, nonmagnetic and probably silica rich, apparently extends for several hundred meters to the east of the western quartz-vein system. Several additional highly resistive, but nonpolarizing features, probably thick nontectonized, dikelike bodies or silica-flooded units, are in the central-southeastern part of the Pistón de Uroy area.

Without direct exploration such as trenching or drilling, the resource potential of the quartz-vein system of Pistón de Uroy is difficult to assess. The characteristics of the vein system are similar to those of the low-sulfide gold-quartz vein model (Berger, 1986). A median grade for the low-sulfide gold-quartz vein model is 16 grams per metric ton, or 16 ppm (Bliss, 1986), a value greater than any determined in the surface samples. Further direct exploration, such as more complete magnetic data and systematic dipole-dipole induced polarization surveys, is needed to more fully evaluate this prospect.

The probability of large concentrations of chromite and nickel and base-metal sulfide minerals in the Pistón de Uroy area is low based on the lack of high concentrations of chromite or sulfide minerals in any samples collected to date or observed in the field. Some rock samples contain anomalous amounts of platinum-group elements, but the distribution and content of these elements have not been determined.

REFERENCES CITED

Alberdi, Margarita, 1988, Informe geológico-geoquímico de la zona El Pistón de Uroy–Abarén, *in* Corporación Venezolana de Guayana, Técnica Minera, C.A., Coordinación General de Prospecciones, Annual Report, 1987, v. 2: Available from Corporación Venezolana de Guayana, Técnica Minera, C.A., Calle Mexico cruce con Calle Estados Unidos, C.C. Chilemex, Piso 1, Puerto Ordaz, Venezuela.

Berger, B.R., 1986, Descriptive model of low-sulfide Au-quartz veins, *in* Cox, D.P., and Singer, D.A., eds., Mineral deposit models: U.S. Geological Survey Bulletin 1693, p. 239.

Bliss, J.D., 1986, Grade and tonnage of low-sulfide Au-quartz veins, *in* Cox, D.P., and Singer, D.A., eds., Mineral deposit models: U.S. Geological Survey Bulletin 1693, p. 239–243.

Contreras, Gloria, and Freites, Dennis, 1989, Informe geológico-geoquímico de las zonas de Canaima-Uroy-Chivao, Río Chicanán, Pistón de Uroy, y Río Cuyuní-Río Uey, *in* Corporación Venezolana de Guayana-Técnica Minera, C.A., Coordinación General de Prospecciones, Annual Report, 1987, v. 1, p. 282–455: Available from Corporación Venezolana de Guayana, Técnica Minera, C.A., Calle Mexico cruce con Calle Estados Unidos, C.C. Chilemex, Piso 1, Puerto Ordaz, Venezuela.

Fraser, D.C., 1969, Contouring of VLF-EM data: Geophysics, v. 34, p. 958.

Grimes, D.J., and Marranzino, A.P., 1968, Direct-current and spark emission spectrographic field methods for semiquantitative analysis of geologic materials: U.S. Geological Survey Circular 591, 6 p.

Meier, A.L., Carlson, R.R., Lichte, F.E., Aruscavage, P.J., and Riddle, G.O., 1988, Determination of the platinum-group elements by fire assay-inductively coupled plasma-mass spectrometry [abs]: The Geochemical Society, V.M. Goldschmidt Conference, Baltimore, May 11–13, 1988.

Mendoza, Vicente, 1977, Evolución tectónica del Escudo de Guayana: Congreso Latinoamericano de Geología, 2nd, Caracas, 1973, Memoria, Publicación Especial 7, v. 3, p. 2237–2270.

Naldrett, A.J., 1981, Platinum-group element deposits, *in* Cabri, L.J., ed., Platinum-group elements—Mineralogy, geology, recovery: Canadian Institute of Mining and Metallurgy Special Volume 23, p. 197–232.

O'Leary, R.M., and Meier, A.L., 1986, Analytical methods used in geochemical exploration, 1984: U.S. Geological Survey Circular 948, 48 p.

Quesada, R.J., and Wynn, J.C., 1990, Métodos geofísicos aplicados a sistemas de vetas de cuarzo aurífero en el Estado Bolívar, Venezuela: Congreso Geofísico Venezolano, 5th, Caracas, 1990, 6 p.

Sumner, J.S., 1976, Principles of induced polarization for geophysical exploration: New York, Elsevier, 277 p.

Tosiani D., Tommaso, and Sifontes G., Ramón, 1989, Asociación de rocas máficas-ultramáficas en la región del Cerro Piedra del Supamo, al sur de El Callao, Estado Bolívar, Venezuela: Congreso Geológico Venezolano, 7th, Barquisimeto, 1989, Memoria, v. 1, p. 163–174.

Zonge, K.L., and Wynn, J.C., 1975, Recent advances and applications in complex resistivity measurements: Geophysics, v. 40, no. 5, p. 851–864.